Eur. Phys. J. C (2020) 80:252
https://doi.org/10.1140/epjc/s10052-020-7817-x

THE EUROPEAN PHYSICAL JOURNAL C

Regular Article - Theoretical Physics

B-decay discrepancies after Moriond 2019

Jason Aebischer[1,a], **Wolfgang Altmannshofer**[2,b], **Diego Guadagnoli**[3,c], **Méril Reboud**[3,d], **Peter Stangl**[3,e], **David M. Straub**[1,f]

[1] Excellence Cluster Universe, Boltzmannstr. 2, 85748 Garching, Germany
[2] Santa Cruz Institute for Particle Physics, University of California, Santa Cruz, CA 95064, USA
[3] Laboratoire d'Annecy-le-Vieux de Physique Théorique, UMR5108, CNRS, 9 Chemin de Bellevue, B.P. 110, 74941 Annecy-le-Vieux Cedex, France

Received: 26 December 2019 / Accepted: 6 March 2020

Abstract Following the updated measurement of the lepton flavour universality (LFU) ratio R_K in $B \to K\ell\ell$ decays by LHCb, as well as a number of further measurements, e.g. R_{K^*} by Belle and $B_s \to \mu\mu$ by ATLAS, we analyse the global status of new physics in $b \to s$ transitions in the weak effective theory at the b-quark scale, in the Standard Model effective theory above the electroweak scale, and in simplified models of new physics. We find that the data continues to strongly prefer a solution with new physics in semi-leptonic Wilson coefficients. A purely muonic contribution to the combination $C_9 = -C_{10}$, well suited to UV-complete interpretations, is now favoured with respect to a muonic contribution to C_9 only. An even better fit is obtained by allowing an additional LFU shift in C_9. Such a shift can be renormalization-group induced from four-fermion operators above the electroweak scale, in particular from semi-tauonic operators, able to account for the potential discrepancies in $b \to c$ transitions. This scenario is naturally realized in the simplified U_1 leptoquark model. We also analyse simplified models where a LFU effect in $b \to s\ell\ell$ is induced radiatively from four-quark operators and show that such a setup is on the brink of exclusion by LHC di-jet resonance searches.

1 Introduction

In recent years, several deviations from standard model (SM) expectations have been building up in B-decay measurements. While each of them could be a first sign of physics beyond the SM, statistical fluctuations or underestimated experimental or theoretical systematic uncertainties cannot be excluded at present. These deviations – or "anomalies" – can be grouped into four categories that have very different experimental and theoretical challenges:

(i) Apparent suppression of various branching ratios of exclusive decays based on the $b \to s\mu\mu$ flavour-changing neutral current (FCNC) transition [1,2]. The uncertainties are dominated by the limited knowledge of the B to light meson hadronic form factors [3–5].
(ii) Deviations from SM expectations in $B \to K^*\mu^+\mu^-$ angular observables [6–9] (also based on the $b \to s\mu\mu$ transition), where form factor uncertainties are much smaller than for the branching ratios, but hadronic uncertainties are nevertheless significant [10,11].
(iii) Apparent deviations from μ-e universality in $b \to s\ell\ell$ transitions in the processes $B \to K\ell\ell$ and $B \to K^*\ell\ell$ (via the μ/e ratios R_K [12] and R_{K^*} [13], respectively). Here the theoretical uncertainties are negligible [14] and the sensitivity is only limited by statistics at present.
(iv) Apparent deviations from τ-μ and τ-e universality in $b \to c\ell\nu$ transitions [15–21]. Uncertainties are dominated by statistics, with non-negligible experimental systematics but small theoretical uncertainties [22–25]. (Note that e-μ universality in $b \to c\ell\nu$ transitions is tested to hold at the percent level [26–28].)

While the deviations in (i) and (ii) could be alleviated by more conservative assumptions on the hadronic uncertainties, it is tantalizing that a simple description in terms of a single non-standard Wilson coefficient of a semi-muonic operator like $(\bar{s}\gamma^\rho P_L b)(\bar{\mu}\gamma_\rho \mu)$ or $(\bar{s}\gamma^\rho P_L b)(\bar{\mu}\gamma_\rho P_L \mu)$ leads to a consistent description of (i), (ii), and (iii), with a best-fit point that improves the fit to the data by more than five standard deviations compared to the SM (for a single degree of freedom)

[a] e-mail: jason.aebischer@tum.de
[b] e-mail: waltmann@ucsc.edu
[c] e-mail: diego.guadagnoli@lapth.cnrs.fr (corresponding author)
[d] e-mail: meril.reboud@lapth.cnrs.fr
[e] e-mail: peter.stangl@lapth.cnrs.fr
[f] e-mail: david.straub@tum.de

Published online: 19 March 2020

[29–34]. Moreover, it was shown that simplified models with a single tree-level mediator can not only explain (i), (ii), and (iii), but even all four categories of deviations simultaneously without violating any other existing constraints [35–40].

Taken together, these observations explain the buzz of activity around these deviations and the anticipation of improved measurements of the theoretically clean ratios R_K and R_{K^*}. The purpose of this article is to examine the status of the tensions after inclusion of a number of updated or newly available measurements, in particular:

- The new measurement of R_K by the LHCb collaboration combining Run-1 data with 2 fb^{-1} of Run-2 data (corresponding to about one third of the full Run-2 data set). The updated measurement finds [41][1]

$$R_K = \frac{\mathrm{BR}(B \to K\mu\mu)}{\mathrm{BR}(B \to Kee)} = 0.846^{+0.060+0.016}_{-0.054-0.014}\,, \quad \text{for } 1.1\,\mathrm{GeV}^2 < q^2 < 6\,\mathrm{GeV}^2\,, \tag{1}$$

  where the first uncertainty is statistical and the second systematic, and q^2 is the dilepton invariant mass squared. The SM predicts lepton flavour universality, i.e. R_K^{SM} is unity with uncertainties that are well below the current experimental sensitivities. While the updated experimental value is closer to the SM prediction than the Run-1 result [12], the reduced experimental uncertainties imply a tension between theory and experiment at the level of 2.5σ, which is comparable to the situation before the update.
- The new, preliminary measurement of R_{K^*} by Belle [42]. Averaged over $B^\pm$ and B^0 decays, the measured R_{K^*} values at low and high q^2 are[2]

$$R_{K^*} = \frac{\mathrm{BR}(B \to K^*\mu\mu)}{\mathrm{BR}(B \to K^*ee)} = \begin{cases} 0.90^{+0.27}_{-0.21} \pm 0.10, & \text{for } 0.1\,\mathrm{GeV}^2 < q^2 < 8\,\mathrm{GeV}^2, \\ 1.18^{+0.52}_{-0.32} \pm 0.10, & \text{for } 15\,\mathrm{GeV}^2 < q^2 < 19\,\mathrm{GeV}^2\,. \end{cases} \tag{2}$$

  Given their sizable uncertainties, these values are compatible with both the SM predictions ($R_{K^*}^{\mathrm{SM}}$ approximately unity) and previous results on R_{K^*} from LHCb [13]

$$R_{K^*} = \frac{\mathrm{BR}(B \to K^*\mu\mu)}{\mathrm{BR}(B \to K^*ee)} = \begin{cases} 0.66^{+0.11}_{-0.07} \pm 0.03, & \text{for } 0.045\,\mathrm{GeV}^2 < q^2 < 1.1\,\mathrm{GeV}^2\,, \\ 0.69^{+0.11}_{-0.07} \pm 0.05, & \text{for } 1.1\,\mathrm{GeV}^2 < q^2 < 6\,\mathrm{GeV}^2\,, \end{cases} \tag{3}$$

  that are in tension with the SM predictions by $\sim 2.5\sigma$ in both q^2 bins.
- One further, important piece of information included in our study is the 2018 measurement of $B_s \to \mu\mu$ by the ATLAS collaboration [46], that we combine with the existing measurements by CMS and LHCb [47–49].
- Finally, we discuss possible connections to the anomalies in the $b \to c\ell\nu$ decays. We take into account the latest updates of R_D and R_{D^*} from Belle [50,51] which, compared to previous results, have central values closer to the SM predictions. Taking into account these updates, the latest world averages from HFLAV are [52]

$$R_D = 0.340 \pm 0.027 \pm 0.013, \qquad R_{D^*} = 0.295 \pm 0.011 \pm 0.008, \tag{4}$$

  corresponding to a combined deviation from the SM by 3.1σ.

In this paper we will explore the implications of all these, as well as other data, to be described in fuller detail in the next section, in the context of global fits to effective-theory new-physics scenarios, whether at the weak scale or at higher scales, identify those scenarios that lead to a good description of the data, and discuss possible realizations in terms of simplified new-physics models.

Our numerical analysis is entirely based on open-source software, notably the global likelihood in Wilson coefficient space provided by the `smelli` package [53], built on `flavio` [54] and `wilson` [55]. As such, our analysis is easily reproducible and modifiable.

The rest of this work is organized as follows.

- In Sect. 2, we describe our statistical approach and the experimental measurements we employ in our numerical analysis.
- In Sect. 3, we perform a global analysis of $b \to s\ell\ell$ transitions, first in the weak effective theory (WET) below the electroweak (EW) scale, then in the SM effective field theory (SMEFT) above the EW scale, which allows us to extend the discussion to the charged-current deviations

[1] In our numerical analysis, we use the full one-dimensional numerical likelihood provided in [41], which is markedly non-Gaussian, rather than symmetrizing the uncertainties in (1).

[2] Belle provides also results for the q^2 bins [0.045, 1.1] GeV^2 and [1.1, 6] GeV^2. The data from these bins is contained in the q^2 bin [0.1, 8] GeV^2 used in our analysis, except for the region between 0.045 GeV^2 and 0.1 GeV^2, which, however, is affected by relatively large theoretical uncertainties due to its proximity to the di-muon kinematical threshold [14]. We also include the q^2 bin [15, 19] GeV^2, which is integrated over a sufficiently large q^2 range to make theoretical predictions in this kinematic region valid. For a detailed discussion of the operator product expansion and violation of quark hadron duality at high q^2, see e.g. [43–45].

and to incorporate constraints from electroweak precision tests and other precision measurements.
- In Sect. 4, we discuss a number of specific simplified new-physics (NP) models that are favoured by the current data, assuming the deviations to be due to NP.
- Sect. 5 contains our conclusions.

2 Setup

Our numerical analysis is based on a global likelihood function in the space of the Wilson coefficients of the WET valid below the EW scale, or the SMEFT valid above it. Theoretical uncertainties (for observables where they cannot be neglected) are treated by computing a covariance matrix of theoretical uncertainties within the SM and combining it with the experimental uncertainties (approximated as symmetrized Gaussians, using the same procedure as in previous studies by some of us [29,30,56–59]). The main assumption in this approach is that the sizes of theory uncertainties are weakly dependent on NP, which we checked for the observables included. This approach was first applied to $b \to s\ell\ell$ transitions in [59]. The theoretical uncertainties in exclusive B-decay observables stem mainly from hadronic form factors, which we take from [3] for B to light vector meson transitions and from [5] for $B \to K$, as well as unknown non-factorizable effects that are parametrized as in [3,54,59] (and are compatible with more sophisticated approaches [10,11]). Additional parametric uncertainties (e.g. from CKM matrix elements) are based on `flavio` v1.3 with default settings [54]. For more details on the statistical approach and the list of observables and measurements included, we refer the reader to [53].

Here we highlight the changes in observables sensitive to $b \to s$ transitions included with respect to the recent global analyses [29,30] by some of us.

- We include the LHCb update of R_K [41] (cf. footnote 1) and the new, preliminary measurement of R_{K^*} by Belle [42]. The Belle results are available for various q^2-bin choices, separately for $B^\pm$ and B^0 decays and in an isospin averaged form. In our numerical analysis we use the $0.1\,\text{GeV}^2 < q^2 < 8\,\text{GeV}^2$ and $15\,\text{GeV}^2 < q^2 < 19\,\text{GeV}^2$ bins, separately for $B^\pm$ and B^0 decays.
- We include the new ATLAS measurement of $B_s \to \mu^+\mu^-$ [46], that we combine with the CMS and LHCb measurements [47–49]. This combination is discussed in detail in Appendix A. Our combination is in slight tension with the SM prediction of $\text{BR}(B_s \to \mu^+\mu^-)$ by approximately 2σ.
- We include the updated LHCb measurement of forward-backward asymmetries in $\Lambda_b \to \Lambda\ell^+\ell^-$ [60] as well as its branching ratio [61]. For the theory predictions of the baryonic decay we follow [62,63].
- Here we are working with the global likelihood described in [53] (i.e. including as many observables sensitive to the Wilson coefficients as possible), while in [29] we focused on observables sensitive to the $b \to s\ell\ell$ transition only. This means e.g. that we also include all the observables sensitive to the $b \to s\gamma$, g dipole transitions studied in [64]. In addition, the global likelihood also includes observables that do not directly depend on the Wilson coefficients of interest but whose theory uncertainties are strongly correlated with those of the directly dependent observables. This is in particular relevant for the $b \to s\mu\mu$ observables. In our figures, we indicate the set of observables consisting of $b \to s\mu\mu$, $b \to s\gamma$, g, and other correlated observables as "$b \to s\mu\mu$ & corr. obs.".
  Like in the previous analysis [30] by some of us, we again include the LFU differences of angular observables[3] $D_{P'_4}$ and $D_{P'_5}$. To this end, we have added them to the global likelihood in version 1.3.0 of the `smelli` package.

3 Effective-theory analysis

Having at hand the global likelihood in the space of NP Wilson coefficients, $L(\vec{C})$, we perform a numerical analysis within effective field theories, the WET and the SMEFT, by discussing in detail certain, well-motivated, one- and two-coefficient scenarios (see e.g. [66]), and collecting a fuller set of them in Appendix E. This analysis proceeds in two steps:

1. We first investigate the Wilson coefficients of the WET at the b-quark mass scale. This analysis can be seen as an update of earlier analyses (see e.g. [29–34]) where our considered scenarios have already been discussed. Such analysis is completely general within our assumed one- or two-coefficient assumption, and barring new particles lighter than the b quark (see e.g. [67–70]).
2. Next, we embed these results into the SMEFT at a scale Λ above the electroweak scale. This is based on the additional assumptions that there are no new particles beneath Λ and that EW symmetry breaking is approximately linear (see e.g. [71]). This allows us to correlate NP effects in $b \to s\ell\ell$, within a general, common formalism, with other sectors like EW precision tests or $b \to c$ transitions (cf. [53,72–74]).

[3] $D_{P'_{4,5}} = P'_{4,5}(B \to K^*\mu^+\mu^-) - P'_{4,5}(B \to K^*e^+e^-)$. The observables $P'_{4,5}$ are defined in [65].

3.1 $b \to s\ell\ell$ observables in the WET

We start by investigating the constraints on NP contributions to the $|\Delta B| = |\Delta S| = 1$ Wilson coefficients of the WET at the b-quark scale $\mu_b \approx m_b$ that we take to be 4.8 GeV. We work with the effective Hamiltonian

$$\mathcal{H}_{\text{eff}}^{bs\ell\ell} = \mathcal{H}_{\text{eff, SM}}^{bs\ell\ell} + \mathcal{H}_{\text{eff, NP}}^{bs\ell\ell}\,, \tag{5}$$

where the first term contains the SM contributions to the Wilson coefficients. The second term reads

$$\mathcal{H}_{\text{eff, NP}}^{bs\ell\ell} = -\mathcal{N}\Big(C_7^{bs}\,O_7^{bs} + C_7^{\prime bs}\,O_7^{\prime bs} + \sum_{\ell=e,\mu}\sum_{i=9,10,S,P}\Big(C_i^{bs\ell\ell}\,O_i^{bs\ell\ell} + C_i^{\prime bs\ell\ell}\,O_i^{\prime bs\ell\ell}\Big)\Big) + \text{h.c.}, \tag{6}$$

with the normalization factor

$$\mathcal{N} = \frac{4G_F}{\sqrt{2}}\,V_{tb}V_{ts}^*\,\frac{e^2}{16\pi^2}\,. \tag{7}$$

The dipole operators are given by[4]

$$O_7^{bs} = \frac{m_b}{e}(\bar{s}\sigma_{\mu\nu}P_R b)F^{\mu\nu}\,, \quad O_7^{\prime bs} = \frac{m_b}{e}(\bar{s}\sigma_{\mu\nu}P_L b)F^{\mu\nu}\,, \tag{8}$$

where $\sigma^{\mu\nu} = \frac{i}{2}[\gamma^\mu, \gamma^\nu]$, and the semi-leptonic operators

$$O_9^{bs\ell\ell} = (\bar{s}\gamma_\mu P_L b)(\bar{\ell}\gamma^\mu \ell)\,, \qquad O_9^{\prime bs\ell\ell} = (\bar{s}\gamma_\mu P_R b)(\bar{\ell}\gamma^\mu \ell)\,, \tag{9}$$

$$O_{10}^{bs\ell\ell} = (\bar{s}\gamma_\mu P_L b)(\bar{\ell}\gamma^\mu\gamma_5 \ell)\,, \qquad O_{10}^{\prime bs\ell\ell} = (\bar{s}\gamma_\mu P_R b)(\bar{\ell}\gamma^\mu\gamma_5 \ell)\,, \tag{10}$$

$$O_S^{bs\ell\ell} = m_b(\bar{s}P_R b)(\bar{\ell}\ell)\,, \qquad O_S^{\prime bs\ell\ell} = m_b(\bar{s}P_L b)(\bar{\ell}\ell)\,, \tag{11}$$

$$O_P^{bs\ell\ell} = m_b(\bar{s}P_R b)(\bar{\ell}\gamma_5 \ell)\,, \qquad O_P^{\prime bs\ell\ell} = m_b(\bar{s}P_L b)(\bar{\ell}\gamma_5 \ell)\,. \tag{12}$$

We have omitted from $\mathcal{H}_{\text{eff, NP}}^{bs\ell\ell}$ semi-leptonic tensor operators, which are not generated at dimension 6 in theories that have SMEFT as EW-scale limit, as well as chromomagnetic and four-quark operators. Even though the latter can contribute via one-loop matrix elements to $b \to s\ell\ell$ processes, their dominant effects typically stem from renormalization group (RG) evolution above the scale μ_b, and we will discuss these effects in the SMEFT framework in the next section. For the same reason, we have constrained the sum over lepton flavours to e and μ: semi-tauonic WET operators can contribute via QED RG mixing, but their direct matrix elements are subleading [75].

[4] The sign of the dipole coefficients $C_7^{(\prime)}$ are fixed by our convention for the covariant derivative $D_\mu\psi = \partial_\mu + ieQ_\psi A_\mu + ig_s T^A G_\mu^A$.

3.1.1 Scenarios with a single Wilson coefficient

We now consider the global likelihood in the space of the above Wilson coefficients. We start with scenarios where only a single NP Wilson coefficient (or a single linear combination motivated by UV scenarios) is nonzero. The best-fit values, 1 and 2σ ranges, and pulls for several such scenarios are listed in Table 1. For the 1D scenarios, the pull in σ is defined as

$$\text{pull} = \sqrt{\Delta\chi^2}, \quad \text{where } -\frac{1}{2}\Delta\chi^2 = \ln L(\vec{0}) - \ln L(\vec{C}_{\text{best fit}})\,. \tag{13}$$

We make the following observations.

- Like in previous analyses, two scenarios stand out, namely a shift to $C_9^{bs\mu\mu}$ by approximately -25% of its SM value ($C_9^{\text{SM}}(\mu_b) \simeq 4.1$), or a shift to the combination $C_9^{bs\mu\mu} = -C_{10}^{bs\mu\mu}$ by approximately -15% of its SM value. However, at variance with previous analyses, it is the second scenario, rather than the first one, to have the largest pull. Given our assumptions about hadronic uncertainties, the pull exceeds 6σ. The main reason why the combination $C_9^{bs\mu\mu} = -C_{10}^{bs\mu\mu}$ performs better is the $\sim 2\sigma$ tension in $\text{BR}(B_s \to \mu\mu)$, which remains unresolved in the $C_9^{bs\mu\mu}$ scenario. We will comment further on this finding in Appendix C.
- New physics in $C_{10}^{bs\mu\mu}$ alone also improves the agreement between theory and data considerably. However, tensions in $B \to K^*\mu\mu$ angular observables remain in this scenario.
- Muonic scenarios with right-handed currents on the quark side, $C_9^{\prime bs\mu\mu}$ and $C_{10}^{\prime bs\mu\mu}$, or the lepton side, $C_9^{bs\mu\mu} = C_{10}^{bs\mu\mu}$, do not lead to a good description of the data.
- Scenarios with NP in $bsee$ Wilson coefficients only, while able to accommodate the discrepancies in $R_{K^{(*)}}$, do not help for the rest of the data. Given the pulls in Table 1, such scenarios are, all in all, less convincing.

The scalar Wilson coefficients $C_{S/P}^{bs\mu\mu}$ and $C_{S/P}^{\prime bs\mu\mu}$ are strongly constrained by the $B_s \to \mu\mu$ decay. In theories that have SMEFT as their EW-scale limit, they satisfy the constraint [77][5]

$$C_S^{bs\mu\mu} = -C_P^{bs\mu\mu}\,, \qquad C_S^{\prime bs\mu\mu} = C_P^{\prime bs\mu\mu}. \tag{14}$$

In this case, they cannot lead to significant modifications in semi-leptonic $b \to s\mu\mu$ transitions [76]. However, the

[5] Discussions of the case where the relations (14) are violated can be found in [71,78]. For a detailed numerical study, including also tensor operators, see Ref. [79].

Table 1 Best-fit values, 1 and 2σ ranges, and pulls (cf. Eq. (13)) between the best-fit point and the SM point for scenarios with NP in a single Wilson coefficient (or Wilson coefficient combination). For the scalar Wilson coefficients, we show the SM-like solution, while also a sign-flipped solution is allowed, see [76]

Coeff.	Best fit	1σ	2σ	Pull
$C_9^{bs\mu\mu}$	-0.97	$[-1.12, -0.81]$	$[-1.27, -0.65]$	5.9σ
$C_9^{\prime bs\mu\mu}$	$+0.14$	$[-0.03, +0.32]$	$[-0.20, +0.51]$	0.8σ
$C_{10}^{bs\mu\mu}$	$+0.75$	$[+0.62, +0.89]$	$[+0.48, +1.03]$	5.7σ
$C_{10}^{\prime bs\mu\mu}$	-0.24	$[-0.36, -0.12]$	$[-0.49, +0.00]$	2.0σ
$C_9^{bs\mu\mu} = C_{10}^{bs\mu\mu}$	$+0.20$	$[+0.06, +0.36]$	$[-0.09, +0.52]$	1.4σ
$C_9^{bs\mu\mu} = -C_{10}^{bs\mu\mu}$	-0.53	$[-0.61, -0.45]$	$[-0.69, -0.37]$	6.6σ
C_9^{bsee}	$+0.93$	$[+0.66, +1.17]$	$[+0.40, +1.42]$	3.5σ
$C_9^{\prime bsee}$	$+0.39$	$[+0.05, +0.65]$	$[-0.27, +0.95]$	1.2σ
C_{10}^{bsee}	-0.83	$[-1.05, -0.60]$	$[-1.28, -0.37]$	3.6σ
$C_{10}^{\prime bsee}$	-0.27	$[-0.57, -0.02]$	$[-0.84, +0.26]$	1.1σ
$C_9^{bsee} = C_{10}^{bsee}$	-1.49	$[-1.79, -1.18]$	$[-2.05, -0.79]$	3.2σ
$C_9^{bsee} = -C_{10}^{bsee}$	$+0.47$	$[+0.33, +0.59]$	$[+0.20, +0.73]$	3.5σ
$\left(C_S^{bs\mu\mu} = -C_P^{bs\mu\mu}\right) \times \text{GeV}$	-0.006	$[-0.009, -0.003]$	$[-0.014, -0.001]$	2.8σ
$\left(C_S^{\prime bs\mu\mu} = C_P^{\prime bs\mu\mu}\right) \times \text{GeV}$	-0.006	$[-0.009, -0.003]$	$[-0.014, -0.001]$	2.8σ

preference of the combination discussed in Appendix A for a suppressed $B_s \to \mu^+\mu^-$ branching ratio means that a destructive interference of these Wilson coefficients with the SM contribution to the leptonic decay can lead to a moderate improvement of the likelihood.

3.1.2 Scenarios with a pair of Wilson coefficients

Next, we consider the likelihood in the space of pairs of Wilson coefficients. The results in Table 1 suggest that NP in both $C_9^{bs\mu\mu}$ and $C_{10}^{bs\mu\mu}$ ought to give an excellent fit to the data. The left plot of Fig. 1 shows the best fit regions in the $C_9^{bs\mu\mu}$-$C_{10}^{bs\mu\mu}$ plane. The orange regions correspond to the 1σ constraints from $b \to s\mu\mu$ observables (including $B_s \to \mu^+\mu^-$) and observables whose uncertainties are correlated with those of the $b \to s\mu\mu$ observables (cf. last point in Sect. 2). In blue we show regions corresponding to the 1σ (right plot) and 2σ (left plot) constraints from the *neutral-current LFU* (NCLFU) observables R_K, R_{K^*}, $D_{P_4'}$, and $D_{P_5'}$. In the right plot, the 1σ constraints from only R_K (purple) and only R_{K^*} (pink) are shown. The combined 1 and 2σ region is shown in red. The dotted contours indicate the situation without the Moriond-2019 results for R_K and R_{K^*}. The best fit point $C_9^{bs\mu\mu} \simeq -0.73$ and $C_{10}^{bs\mu\mu} \simeq 0.40$ has a $\sqrt{\Delta\chi^2} = 6.6$, which, corrected for the two degrees of freedom, corresponds to a pull of 6.3σ. In this scenario a slight tension between R_K and R_{K^*} remains, as it predicts $R_K \simeq R_{K^*}$ while the data seems to indicate $R_K > R_{K^*}$. In addition, there is also a slight tension between the fit to NCLFU observables and the fit to $b \to s\mu\mu$ ones, especially in the $C_9^{bs\mu\mu}$ direction.

Overall, we find a similarly good fit of the data in a scenario with NP in $C_9^{bs\mu\mu}$ and $C_9^{\prime bs\mu\mu}$. The scenario is shown in the right plot of Fig. 1. The best fit values for the Wilson coefficients are $C_9^{bs\mu\mu} \simeq -1.06$ and $C_9^{\prime bs\mu\mu} \simeq 0.47$. The $\sqrt{\Delta\chi^2} = 6.4$ corresponds to a pull of 6.0σ. Interestingly, in this scenario a non-zero $C_9^{\prime bs\mu\mu}$ is preferred at the 2σ level. The right-handed quark current allows one to accommodate the current experimental results for the LFU ratios, $R_K > R_{K^*}$. This scenario cannot address the tension in $\text{BR}(B_s \to \mu^+\mu^-)$. It predicts $\text{BR}(B_s \to \mu^+\mu^-) = \text{BR}(B_s \to \mu^+\mu^-)_{\text{SM}}$.

Other two-coefficient scenarios (including dipole coefficients, scalar coefficients, and electron specific semileptonic coefficients) are discussed in Appendix E.

3.1.3 Universal vs. non-universal Wilson coefficients

In view of the updated $R_{K^{(*)}}$ measurements, which are closer to the SM prediction than the Run-1 results, our fit in $C_9^{bs\mu\mu}$ and $C_{10}^{bs\mu\mu}$ shows a tension between the fit to NCLFU observables and the fit to $b \to s\mu\mu$ ones, especially in the $C_9^{bs\mu\mu}$ direction. Therefore, it is interesting to investigate whether lepton flavour universal new physics that mostly affects $b \to s\mu\mu$ observables but none of the NCLFU observables is preferred by the global analysis. In Fig. 2 we show the likelihood in the space of a LFU contribution to C_9 vs. a purely muonic contribution to the linear combination $C_9 = -C_{10}$, i.e. we consider a two-parameter scenario where the total NP

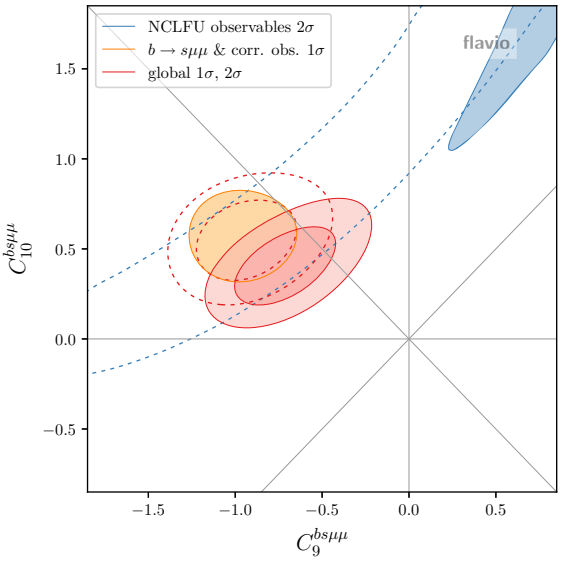

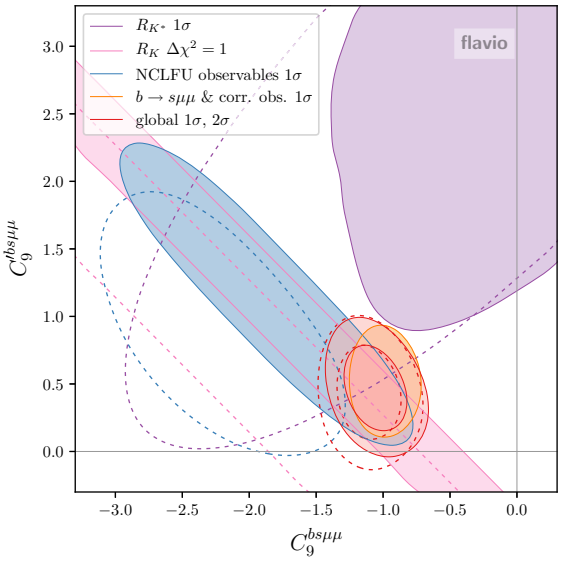

Fig. 1 Likelihood contours of the global fit and several fits to subsets of observables (see text for details) in the plane of the WET Wilson coefficients $C_9^{bs\mu\mu}$ and $C_{10}^{bs\mu\mu}$ (left), and $C_9^{bs\mu\mu}$ and $C_9^{\prime bs\mu\mu}$ (right). Solid (dashed) contours include (exclude) the Moriond-2019 results for R_K and R_{K^*}. As R_K only constrains a single combination of Wilson coefficients in the right plot, its 1σ contour corresponds to $\Delta\chi^2 = 1$. For the other fits, 1 and 2σ contours correspond to $\Delta\chi^2 \approx 2.3$ and 6.2, respectively

Wilson coefficients are given by[6]

$$C_9^{bs\mu\mu} = \Delta C_9^{bs\mu\mu} + C_9^{\text{univ.}}, \tag{15}$$

$$C_9^{bsee} = C_9^{bs\tau\tau} = C_9^{\text{univ.}}, \tag{16}$$

$$C_{10}^{bs\mu\mu} = -\Delta C_9^{bs\mu\mu}, \tag{17}$$

$$C_{10}^{bsee} = C_{10}^{bs\tau\tau} = 0. \tag{18}$$

The best fit values in this scenario are $C_9^{\text{univ.}} = -0.49$ and $\Delta C_9^{bs\mu\mu} = -0.44$ with a $\sqrt{\Delta\chi^2} = 6.8$ that corresponds to a pull of 6.5σ. The updated values of $R_{K^{(*)}}$ favour a nonzero lepton flavour universal contribution to C_9 in this scenario.

One qualification is in order at this point. It is conceivable that a new effect in C_9, and all the more the $C_9^{\text{univ.}}$ contribution discussed above, is mimicked by a hadronic SM effect that couples to the lepton current via a virtual photon, for example charm-loop effects at low q^2 and resonance effects at high q^2, see e.g. [81–83]. In our analysis, this possibility is taken into account in the uncertainty attached to the relevant observables that contribute to the (yellow) $b \to s\mu\mu$ region in Fig. 2. Specifically, non-factorizable effects are parameterized as in [59] which, at 1σ, envelops the hadronic effects identified in [10,84]. With such 'standard' procedure (adopted e.g. also in [85–87]), the global fit in Fig. 2 requires a non-SM $C_9^{\text{univ.}}$ shift at slightly more than 1σ.

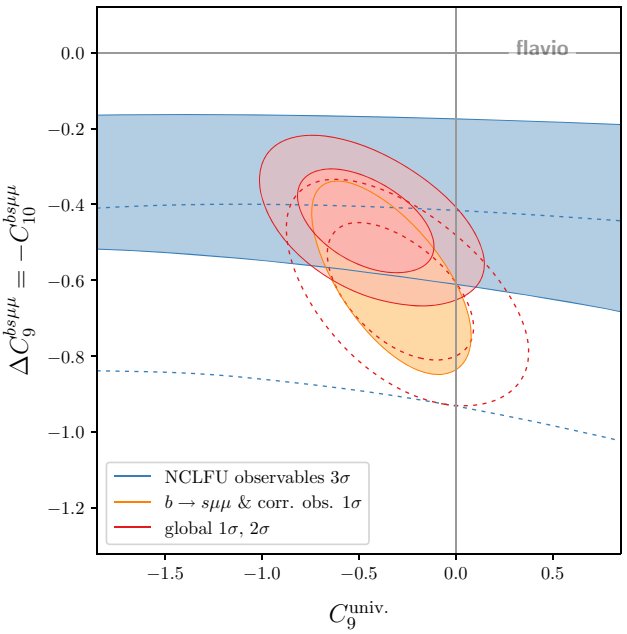

Fig. 2 Likelihood contours from NCLFU observables ($R_{K^{(*)}}$ and $D_{P'_{4,5}}$), $b \to s\mu\mu$ observables, and the global fit in the plane of a lepton flavour universal contribution to $C_9^{\text{univ.}} \equiv C_9^{bs\ell\ell}$, $\forall\ell$, and a muon-specific contribution to the linear combination $C_9 = -C_{10}$ (see text for details). Solid (dashed) contours include (exclude) the Moriond-2019 results for R_K and R_{K^*}

[6] Such decomposition was adopted for the first time in [80], to which we refer the reader for additional scenarios beyond the one we consider. We note that a shift in $C_{10}^{\text{univ.}}$ would not produce a good overall fit. This may be appreciated from Fig. 1 (left). A $C_{10}^{\text{univ.}}$ shift would only move the (yellow) $b \to s\mu\mu$ region vertically, hence it would not help reach better agreement with the (blue) NCLFU region. We therefore set non-muonic C_{10} contributions to zero for simplicity.

More conservative assumptions about the aforementioned hadronic uncertainties would not impact any of the observables that have been updated since Moriond 2017, when some of us performed a detailed study [29] of enlarged hadronic uncertainties, building on a similar study in Ref. [59]. By assuming non-form-factor hadronic uncertainties that are doubled with respect to the assumption denoted above as 'standard' and used in the present study, the global fit would be compatible with a vanishing NP contribution to $C_9^{\text{univ.}}$ at the 1σ level.

With the above qualification in mind, in the following Sections we will address the question whether the above scenario, with a muon-specific contribution, $\Delta C_9^{bs\mu\mu} = -C_{10}^{bs\mu\mu}$, plus a universal contribution, $C_9^{\text{univ.}}$, can be justified from the UV point of view, assuming that both contributions are due to new physics. We start from a general discussion of how such contributions can arise in the SMEFT (Sect. 3.2) and discuss in detail how a lepton-flavour universal NP effect, $C_9^{\text{univ.}}$, can arise from RG effects in Sect. 3.3.

3.2 The global picture in the SMEFT

In this Section we summarize the interpretation of the above results within the SMEFT. In contrast to the discussion in WET at the b-quark scale, more Wilson coefficients become relevant in SMEFT due to RG mixing above [88–90] and below [91,92] the EW scale. Due to the pattern of Wilson coefficients preferred by the global fit, we focus on SMEFT Wilson coefficients that either contribute to the semimuonic Wilson coefficients in the form $C_9^{bs\mu\mu} = -C_{10}^{bs\mu\mu}$ or induce a LFU effect in $C_9^{bs\ell\ell}$. Our notation in the following will be such that ℓ refers to leptons below the EW scale and l to the lepton doublets above the EW scale. Furthermore, we will work in a basis where generation indices for RH quarks are taken to coincide with the mass basis [93], which can be done without loss of generality.

The direct matching contributions to $C_{9,10}$ at the EW scale are well known [94,95],

$$2\mathcal{N}\, C_9^{bs\ell_i\ell_i} = [C_{qe}]_{23ii} + [C_{lq}^{(1)}]_{ii23} + [C_{lq}^{(3)}]_{ii23} - \zeta c_Z\,, \tag{19}$$

$$2\mathcal{N}\, C_{10}^{bs\ell_i\ell_i} = [C_{qe}]_{23ii} - [C_{lq}^{(1)}]_{ii23} - [C_{lq}^{(3)}]_{ii23} + c_Z\,, \tag{20}$$

where the normalization factor $\mathcal{N}$ is defined in (7), the Z penguin coefficient c_Z is

$$c_Z = [C_{\varphi q}^{(1)}]_{23} + [C_{\varphi q}^{(3)}]_{23}\,, \tag{21}$$

and $\zeta = 1 - 4s_w^2 \approx 0.08$ is the accidentally suppressed vector coupling of the Z to charged leptons. Using the notation of [96], the corresponding operators are given by

$$[O_{qe}]_{23ii} = (\bar{q}_2\gamma_\mu q_3)(\bar{e}_i\gamma^\mu e_i)\,, \tag{22}$$

$$[O_{lq}^{(1)}]_{ii23} = (\bar{l}_i\gamma_\mu l_i)(\bar{q}_2\gamma^\mu q_3)\,,$$

$$[O_{lq}^{(3)}]_{ii23} = (\bar{l}_i\gamma_\mu \tau^I l_i)(\bar{q}_2\gamma^\mu \tau^I q_3)\,, \tag{23}$$

$$[O_{\varphi q}^{(1)}]_{23} = (\varphi^\dagger i\overleftrightarrow{D}_\mu \varphi)(\bar{q}_2\gamma^\mu q_3)\,,$$

$$[O_{\varphi q}^{(3)}]_{23} = (\varphi^\dagger i\overleftrightarrow{D}^I_\mu \varphi)(\bar{q}_2\gamma^\mu \tau^I q_3)\,, \tag{24}$$

where q_i, and l_i are the left-handed $SU(2)_L$ doublet quarks and leptons and e_i are the right-handed lepton singlets, φ is the SM Higgs doublet, and τ^I are the Pauli matrices.

Equations (19) and (20) highlight the well-known fact that a LFU contribution to $C_{9,10}$ induced by the SMEFT coefficients $[C_{\varphi q}^{(1,3)}]_{23}$ (yielding a flavour-changing $\bar{s}bZ$ coupling) is not preferred by the data since it leads to $|C_{10}^{bs\ell_i\ell_i}| \gg |C_9^{bs\ell_i\ell_i}|$. Likewise, the coefficient $[C_{qe}]_{23ii}$ alone leads to $C_9^{bs\ell_i\ell_i} = C_{10}^{bs\ell_i\ell_i}$ that is in poor agreement with the data as well. Thus, if the dominant NP effect in $C_{9,10}^{bs\mu\mu}$ does *not* stem from an RG effect but a direct matching contribution, it must involve one of the SMEFT Wilson coefficients $[C_{lq}^{(1,3)}]_{2223}$. In addition to the dominant $[C_{lq}^{(1,3)}]_{2223}$ contribution, there can also be contributions from other Wilson coefficients. However, such additional contributions need, in general, be small (see e.g. [97]).

Apart from the direct matching contributions, additional SMEFT Wilson coefficients can induce a contribution to C_9 at the b mass scale through RG evolution above or below the EW scale, as pictured in Fig. 3. In view of the size of the effect preferred by the data, we can identify three qualitatively different effects that can play a role:

- Wilson coefficients $[C_{eu}]_{2233}$ and $[C_{lu}]_{2233}$ of the ditop-dimuon operators $[O_{eu}]_{2233} = (\bar{e}_2\gamma_\mu e_2)(\bar{u}_3\gamma^\mu u_3)$ and $[O_{lu}]_{2233} = (\bar{l}_2\gamma_\mu l_2)(\bar{u}_3\gamma^\mu u_3)$ that induce a contribution to $C_9^{bs\mu\mu}$ from electroweak running above the EW scale. However, this solution is seriously challenged by EW precision tests [73].
- Wilson coefficients $[C_{lq}^{(1,3)}]_{3323}$ or $[C_{qe}]_{2333}$ of semitauonic operators $[O_{lq}^{(1)}]_{3323}$, $[O_{lq}^{(3)}]_{3323}$, or $[O_{qe}]_{2333}$ defined in (22) and (23), that induce a LFU contribution to $C_9^{bs\ell\ell}$ from gauge-induced running both above and below the EW scale [75,98].
- Four-quark operators (defined below in Sect. 3.3.2) that also induce a LFU contribution to $C_9^{bs\ell\ell}$ analogously to the semitauonic ones [99].

The case of semitauonic operators is particularly interesting as it potentially allows for a simultaneous explanation of the anomalies in neutral-current $b \to s$ transitions and in

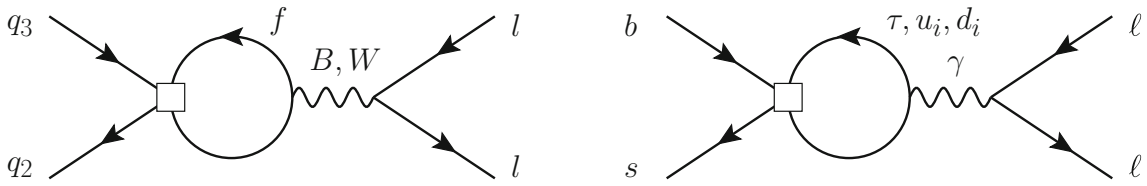

Fig. 3 Diagrams inducing a contribution to C_9 through RG running above (left panel) and below (right panel) the EW scale. A sizeable contribution to C_9 is obtained when $f = u_{1,2}, d_{1,2,3}$ or l_3, see text for details

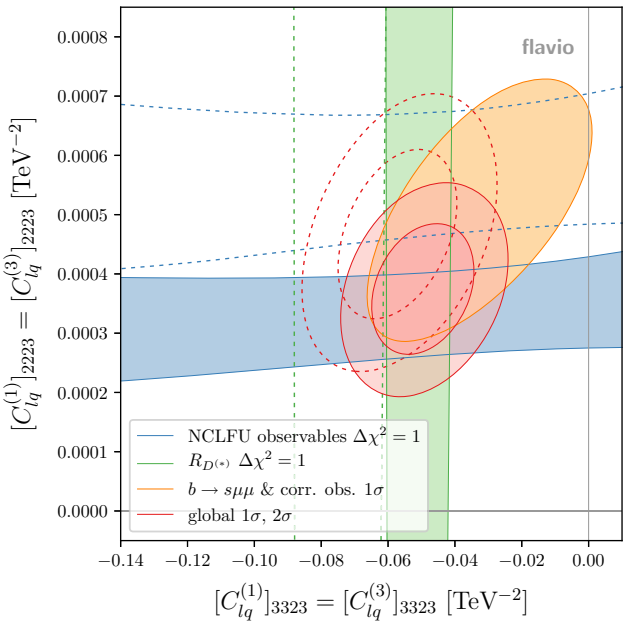

Fig. 4 Likelihood contours from $R_{D^{(*)}}$, NCLFU observables ($R_{K^{(*)}}$ and $D_{P'_{4,5}}$), and $b \to s\mu\mu$ observables in the space of the two SMEFT Wilson coefficients $[C_{lq}^{(1)}]_{3323} = [C_{lq}^{(3)}]_{3323}$ and $[C_{lq}^{(1)}]_{2223} = [C_{lq}^{(3)}]_{2223}$ at 2 TeV. All other Wilson coefficients are assumed to vanish at 2 TeV. Solid (dashed) contours include (exclude) the Moriond-2019 results for R_K, R_{K^*}, R_D, and R_{D^*}. For sets of data that effectively constrain only a single Wilson coefficient (namely $R_{D^{(*)}}$ and NCLFU observables), 1σ contours correspond to $\Delta\chi^2 = 1$. For the other data ($b \to s\mu\mu$ and the global likelihood), 1 and 2σ contours correspond to $\Delta\chi^2 \approx 2.3$ and 6.2, respectively

charged-current $b \to c$ transitions involving taus [53,98]. We now discuss these two possibilities in turn, from an effective-theory point of view. Specific realizations in terms of simplified models will be discussed in Sect. 4.

3.3 LFU C_9 from RG effects

3.3.1 Semi-tauonic operators

Intriguingly, a large value for $[C_{lq}^{(3)}]_{3323}$, that can explain the hints for LFU violation in charged-current $b \to c$ transitions (R_D and R_{D^*}), also induces a LFU effect in C_9 that goes in the right direction to solve the $b \to s\mu\mu$ anomalies in branching ratios and angular observables. An additional contribution to $[C_{lq}^{(a)}]_{2223}$ ($a = 1$ or 3) of similar size can accommodate the deviations in R_K and R_{K^*}. Since the linear combination $[C_{lq}^{(1)}]_{3323} - [C_{lq}^{(3)}]_{3323}$ generates a sizable contribution to $B \to K^{(*)}\nu\bar{\nu}$ decays [95] that is constrained by B-factory searches for these modes, such models are only viable if the semitauonic singlet and triplet Wilson coefficients are approximately equal.[7] For reference, the leading-log contribution from $[C_{lq}^{(1,3)}]_{3323}$ to C_9 due to gauge mixing is given by[8] [98]

$$C_9 \approx -\frac{\sqrt{2}}{G_F V_{tb} V_{ts}^*} \frac{1}{6} \log\left(\frac{\Lambda^2}{m_b^2}\right) \left([C_{lq}^{(1)}]_{3323} + [C_{lq}^{(3)}]_{3323}\right). \tag{25}$$

Figure 4 shows the likelihood contributions from $R_{D^{(*)}}$, NCLFU observables, $b \to s\mu\mu$ observables, and the global likelihood in the space of the two Wilson coefficients $[C_{lq}^{(1)}]_{3323} = [C_{lq}^{(3)}]_{3323}$ and $[C_{lq}^{(1)}]_{2223} = [C_{lq}^{(3)}]_{2223}$ at the renormalization scale $\mu = 2$ TeV. It is interesting to note that before the Moriond 2019 updates (indicated by the dashed contours), for a purely muonic solution with $[C_{lq}^{(1,3)}]_{3323} = 0$ (corresponding to the vertical axis), the best-fit values for NCLFU and $b \to s\mu\mu$ data were in perfect agreement with each other (even though $R_{D^{(*)}}$ cannot be explained in this case). Including the $R_{K^{(*)}}$ updates, the best-fit point of the NCLFU and $b \to s\mu\mu$ data instead lies in the region with non-zero semitauonic Wilson coefficients, just as required to explain the $R_{D^{(*)}}$ anomalies. In fact, the agreement between the 1σ regions for $R_{K^{(*)}}$ & $D_{P'_{4,5}}$, $R_{D^{(*)}}$, and $b \to s\mu\mu$ *improves* compared to the case without the $R_{K^{(*)}}$ updates. We note that a further improvement of the fit is achieved by taking into account the Moriond 2019 update of $R_{D^{(*)}}$ by Belle [50,51], which moves the 1σ region for $R_{D^{(*)}}$ slightly closer to the SM value, exactly to the region where the contours of NCLFU and $b \to s\mu\mu$ observables overlap. The best fit values in this scenario are $[C_{lq}^{(1,3)}]_{3323} = -5.0 \times 10^{-2}$ TeV^{-2}

[7] Note that exact equality is not preserved by the RG evolution in SMEFT.

[8] The analytic expression in Eq. (25) includes only the contribution from the photon-penguin diagram. An additional Z-penguin diagram gives a suppressed contribution [98] and is not included. In our numerical analysis, we take into account the full SMEFT RG effects including also the suppressed contributions.

Table 2 Predictions for LFU ratios, angular observables, and branching ratios in B and B_s decays from the global likelihood in the space of SMEFT Wilson coefficients $[C_{lq}^{(1)}]_{3323} = [C_{lq}^{(3)}]_{3323}$ and $[C_{lq}^{(1)}]_{2223} = [C_{lq}^{(3)}]_{2223}$ (cf. Fig. 4) and corresponding SM predictions

Observable	1σ	2σ	SM
$R_{K^*}^{[0.045,1.1]}$	$0.88^{+0.01}_{-0.01}$	[0.86, 0.90]	0.926 ± 0.004
$R_{K^*}^{[1.1,6.0]}$	$0.81^{+0.04}_{-0.04}$	[0.73, 0.89]	0.9964 ± 0.0006
$R_{K^*}^{[0.1,8.0]}$	$0.83^{+0.04}_{-0.03}$	[0.77, 0.90]	0.995 ± 0.002
$R_{K^*}^{[15,19]}$	$0.79^{+0.04}_{-0.04}$	[0.71, 0.88]	0.99807 ± 0.00004
$R_K^{[1.0,6.0]}$	$0.80^{+0.04}_{-0.04}$	[0.71, 0.88]	1.0008 ± 0.0003
$R_\phi^{[1.0,6.0]}$	$0.81^{+0.04}_{-0.04}$	[0.73, 0.89]	0.9970 ± 0.0003
$\langle P_5' \rangle^{[4.0,6.0]}$	$-0.58^{+0.13}_{-0.12}$	$[-0.82, -0.33]$	-0.763 ± 0.072
R_D	$0.34^{+0.01}_{-0.01}$	[0.32, 0.37]	0.303 ± 0.006
R_{D^*}	$0.29^{+0.01}_{-0.01}$	[0.27, 0.31]	0.255 ± 0.004
$\overline{\text{BR}}(B_s \to \mu^+\mu^-)$	$2.98^{+0.20}_{-0.19} \times 10^{-9}$	$[2.60, 3.38] \times 10^{-9}$	$(3.67 \pm 0.16) \times 10^{-9}$
$\text{BR}(B^\pm \to K^\pm\tau^+\tau^-)$	$3.05^{+1.78}_{-1.06} \times 10^{-5}$	$[1.01, 6.47] \times 10^{-5}$	$(1.66 \pm 0.19) \times 10^{-7}$
$\overline{\text{BR}}(B_s \to \tau^+\tau^-)$	$1.41^{+0.80}_{-0.47} \times 10^{-4}$	$[0.52, 2.94] \times 10^{-4}$	$(7.78 \pm 0.33) \times 10^{-7}$

and $[C_{lq}^{(1,3)}]_{2223} = 3.9 \times 10^{-4}$ TeV^{-2} with a $\sqrt{\Delta\chi^2} = 8.1$ that corresponds to a pull of 7.8σ. The pull is considerably larger in the present scenario than in those discussed in Sect. 3.1 since it can also explain discrepancies in $b \to c$ transitions. Plugging the above values into Eq. (25) one finds a good agreement with the universal-C_9 shift found in Sect. 3.1.3.

It is interesting to use the global fit in this scenario as the basis for predictions of several observables that are sensitive to the Wilson coefficients $[C_{lq}^{(1,3)}]_{3323}$ and $[C_{lq}^{(1,3)}]_{2223}$ and are supposed to be measured with higher precision in the near future. We collect predictions for LFU ratios, angular observables, and branching ratios in B and B_s decays in Table 2.

In the previous discussion we have focused on the global consistency between NCLFU and $b \to s\mu\mu$ data, which after Moriond 2019 would call for a universal C_9 contribution, which in turn is quantitatively consistent with the NP contribution demanded by $R_{D^{(*)}}$. An interesting question[9] is the comparison of this SMEFT scenario with the SM when taking into account LFU data alone, i.e. omitting $b \to s\mu\mu$ data. This question is of interest e.g. because LFU data are deemed the theoretically cleanest.

To address this question we performed a fit taking into account only LFU observables in $b \to s\ell\ell$ and $b \to c\ell\nu$. The two sets of observables are effectively orthogonal and therefore lead to fully consistent best-fit regions in the plane of the Wilson coefficients $[C_{lq}^{(1)}]_{3323} = [C_{lq}^{(3)}]_{3323}$ and $[C_{lq}^{(1)}]_{2223} = [C_{lq}^{(3)}]_{2223}$, for both pre- and post-Moriond 2019 data. With the Moriond 2019 updates we find best fit values of the Wilson coefficients $[C_{lq}^{(1,3)}]_{3323} = -5.0 \times 10^{-2}$ TeV^{-2} and $[C_{lq}^{(1,3)}]_{2223} = 3.4 \times 10^{-4}$ TeV^{-2} corresponding to $\sqrt{\Delta\chi^2} = 5.3$ and a pull of 4.9σ.

[9] We thank the Referee for the suggestion.

3.3.2 *Four-quark operators*

Four-quark SMEFT operators can induce a LFU contribution to C_9 through gauge-induced RG running above and below the EW scale from diagrams like in Fig. 3. Since the flavour-changing quark current in O_9 is left-handed, these operators must contain at least two q fields and the other current must be a $SU(3)_c$ singlet. Neglecting CKM mixing (i.e. to zeroth order in the Cabibbo angle), the following operators could thus play a role:

$$[O_{qq}^{(1)}]_{23ii} = (\bar{q}_2\gamma_\mu q_3)(\bar{q}_i\gamma^\mu q_i)\,,$$
$$[O_{qq}^{(3)}]_{23ii} = (\bar{q}_2\gamma_\mu \tau^I q_3)(\bar{q}_i\gamma^\mu \tau^I q_i)\,, \tag{26}$$
$$[O_{qu}^{(1)}]_{23ii} = (\bar{q}_2\gamma_\mu q_3)(\bar{u}_i\gamma^\mu u_i)\,,$$
$$[O_{qd}^{(1)}]_{23ii} = (\bar{q}_2\gamma_\mu q_3)(\bar{d}_i\gamma^\mu d_i)\,. \tag{27}$$

In the discussion to follow, we will consider each one of the above operators, and discuss whether they can produce *at all* a LFU C_9 contribution of the right size, in the light of all known low-energy constraints.

- $[O_{qq}^{(1)}]_{2333}$ and $[O_{qu}^{(1)}]_{2333}$ induce a LFU contribution to C_{10} that is much bigger than the one in C_9 by a factor $(1 - 4s_W^2)^{-1} \sim 13$ through a $\bar{s}bZ$ coupling generated by a top-quark loop, so they cannot explain the data.
- In the basis where the down-type quark mass matrix is diagonal, all the $[O_{qq}^{(a)}]_{23ii}$ operators lead to enormous NP contributions to CP violation in D^0-$\bar{D}^0$ mixing that are excluded by observations [52]. Note that this happens even for real SMEFT Wilson coefficients since the CKM rotation between the mass basis for left-handed down-

type quarks (relevant for $b_L \to s_L$ transitions) and up-type quarks (relevant for $u_L \leftrightarrow c_L$) is itself CP violating. For example, the operator $[O_{qq}^{(1)}]_{2311}$ contributes to D^0-$\bar{D}^0$ mixing through the operator $C_D(\bar{u}c)_{V-A}(\bar{u}c)_{V-A}$ with $C_D \sim \lambda^8[C_{qq}^{(1)}]_{2311}$ where λ is the Cabibbo angle. For a typical value of $[C_{qq}^{(1)}]_{2311} \sim (1\text{ TeV})^{-2}$ we find $C_D \sim (10^3\text{ TeV})^{-2}$, which exceeds existing bounds [100] by an order of magnitude. Working instead in the basis where the up-type quark mass matrix is diagonal[10] and only using operators $[\hat{O}_{qq}^{(a)}]_{iijj}$ that do not contribute to D^0-$\bar{D}^0$ mixing, it turns out that all these operators either generate excessive contributions to CP violation in K^0-$\bar{K}^0$ mixing[11] or do not generate an appreciable contribution to C_9.
- $[O_{qu}^{(1)}]_{2311}$ and $[O_{qd}^{(1)}]_{2311}$ can induce a NP contribution to ϵ'/ϵ [101,102] (i.e. direct CP violation in $K^0 \to \pi\pi$) through RG running above the EW scale, but for a low enough scale they can lead to a visible effect in C_9 without violating this bound.
- $[O_{qd}^{(1)}]_{2322}$ can induce a NP contribution to ΔM_s, the mass difference in the B_s-$\bar{B}_s$ system, through RG running above the EW scale, but for a low enough scale it can lead to a visible effect in C_9 without violating this bound.
- An effect in C_9 generated by $[O_{qu}^{(1)}]_{2322}$ and $[O_{qd}^{(1)}]_{2333}$ is not strongly constrained from the point of view of low-energy data, and is thus allowed from these data alone. We will discuss possible contributions to these operators from the point of view of UV completions in Sect. 4.2, see Eqs. (43)–(44).

To summarize, a LFU contribution to C_9 could, barring cancellations, be generated by the SMEFT Wilson coefficients

$$[C_{qu}^{(1)}]_{2311},\quad [C_{qu}^{(1)}]_{2322},\quad [C_{qd}^{(1)}]_{2311},\quad [C_{qd}^{(1)}]_{2322},\quad [C_{qd}^{(1)}]_{2333}. \tag{28}$$

The generic size of these Wilson coefficients required for a visible effect in C_9 is in the ballpark of $1/\text{TeV}^2$.

Consequently, realistic model implementations of such an effect have to rely on tree-level mediators with sizeable couplings to quarks and masses potentially in the reach of direct production at LHC. We will discuss such simplified models in Sect. 4.2.

[10] Operators and couplings in such up-aligned basis are here and henceforth denoted with a hat.

[11] As well known, see [100] for the most recent study, this constraint is violated for new-physics scales below $O(10^4)$ TeV, which is way above the scale required by B discrepancies.

4 Simplified new-physics models

In this section we consider simplified models with a single tree-level mediator multiplet giving rise to the Wilson coefficient patterns that are in agreement with the above findings in the EFT.

In Sect. 4.1, we consider the U_1 vector leptoquark, transforming as $(\mathbf{3},\mathbf{1})_{2/3}$ under the SM gauge group [35,38,103–110], that is known to be the only viable simultaneous single-mediator explanation of the $R_{K^{(*)}}$ and $R_{D^{(*)}}$ anomalies [37,111–115]. Since it generates the semitauonic operators discussed in Sect. 3.3.1, it can also generate a LFU contribution to C_9.

In Sect. 4.2, we discuss realizations of LFU contributions to C_9 via RG effects from four-quark operators as discussed in Sect. 3.3.2. We will show that there is a single viable mediator, a scalar transforming as $(\mathbf{8},\mathbf{2})_{1/2}$ under the SM gauge group, and that it is strongly constrained by LHC di-jet searches.

4.1 Explaining the data by a single mediator: the U_1 leptoquark solution

As anticipated above, the only single mediator that can yield non-zero values for $[C_{lq}^{(1)}]_{3323} = [C_{lq}^{(3)}]_{3323}$ and $[C_{lq}^{(1)}]_{2223} = [C_{lq}^{(3)}]_{2223}$ is the U_1 vector leptoquark, which transforms as $(\mathbf{3},\mathbf{1})_{2/3}$ under the SM gauge group. We define its couplings to the left-handed SM fermion doublets q and l as

$$\mathcal{L}_{U_1} \supset g_{lq}^{ji}\left(\bar{q}^i\gamma^\mu l^j\right)U_\mu + \text{h.c.} \tag{29}$$

From the tree-level matching at the scale $\Lambda = M_U$, one finds

$$[C_{lq}^{(1)}]_{ijkl} = [C_{lq}^{(3)}]_{ijkl} = -\frac{g_{lq}^{jk}\,g_{lq}^{il*}}{2M_U^2}. \tag{30}$$

Consequently, for a given leptoquark mass, a τ-channel contribution to $R_{D^{(*)}}$ depends only on g_{lq}^{32} and g_{lq}^{33}, while a μ-channel contribution to $R_{K^{(*)}}$ depends only on g_{lq}^{22} and g_{lq}^{23}.

We perform an analysis at leading-logarithm accuracy, i.e. we take into account the one-loop RG running and mixing and perform the matching at tree level. As has been shown in [98,116], the one-loop matching of a simplified[12] U_1 leptoquark model would lead to

- a 13% enhancement [116] of the tree-level contribution to semileptonic operators,
- contributions to leptonic operators inducing $\tau \to \mu\bar{\nu}\nu$,

[12] Note that one-loop matching results are very model dependent. In a full model, the size of the contributions listed below can change significantly and additional contributions can be present.

- contributions to semi-leptonic operators inducing $B \to K^{(*)}\bar{\nu}\nu$,
- contributions to electric and chromomagnetic dipole operators in the WET.

Except for the last point, all of these contributions either only correct an already included tree-level result or are small compared to the current experimental sensitivity or compared to RG effects that contribute to the same operators (cf. [98]). We thus neglect them in the following. On the other hand, the one-loop matching contributions to the electric and chromomagnetic dipole operators can lead to relevant shifts in the Wilson coefficient C_7 at the b-quark scale, which are constrained by measurements of $b \to s\gamma$ observables (cf. [64]). In order to be sensitive to this possibly important effect, we will take the one-loop matching contributions to the SMEFT quark-dipole operators into account. ‘ as [96]

$$[O_{dB}]_{ij} = (\bar{q}_i \sigma^{\mu\nu} d_j)\varphi B_{\mu\nu}\,,$$
$$[O_{dW}]_{ij} = (\bar{q}_i \sigma^{\mu\nu} d_j)\tau^I \varphi W^I_{\mu\nu}\,, \tag{31}$$
$$[O_{dG}]_{ij} = (\bar{q}_i \sigma^{\mu\nu} T^A d_j)\varphi G^A_{\mu\nu}\,. \tag{32}$$

The matching result depends on the couplings of the U_1 vector leptoquark to the SM gauge bosons, which can be written as

$$\mathcal{L}_{U_1} \supset -\frac{1}{2}U^\dagger_{\mu\nu}U^{\mu\nu} + ig_s k_s U^\dagger_\mu T^A U_\nu G^{A,\mu\nu} + ig' \frac{2}{3} k_Y U^\dagger_\mu U_\nu B^{\mu\nu}\,, \tag{33}$$

where

$$U_{\mu\nu} = D_\mu U_\nu - D_\nu U_\mu \quad \text{with} \quad D_\mu = \partial_\mu + ig_s T^A G^A_\mu + ig' \frac{2}{3} B_\mu. \tag{34}$$

These couplings are determined by SM gauge invariance except for the two parameters k_s and k_Y. In the following, we make the choice $k_s = k_Y = 1$, which leads to a cancellation of divergent tree-level diagrams in U_1-gluon and U_1-B-boson scattering [117] and further avoids logarithmically divergent contributions to the dipole operators [37], making them finite and gauge independent. We note that $k_s = k_Y = 1$ is automatically satisfied in any model in which the U_1 leptoquark stems from the spontaneous breaking of a gauge symmetry but can also be realized for a composite U_1 [118].

We perform the one-loop matching to quark-dipole operators at the scale $\Lambda = M_U$ by computing the diagrams shown in Fig. 5. Working in the basis in which the down-type Yukawa matrix is diagonal, and using the conventions mentioned above, we find the Wilson coefficients of the EW dipole operators

$$[C_{dW}]_{23} = Y_b \frac{g}{16\pi^2}\left(\frac{1}{6}\right)\frac{g^{i2}_{lq}\, g^{i3*}_{lq}}{M_U^2},$$
$$[C_{dW}]_{32} = Y_s \frac{g}{16\pi^2}\left(\frac{1}{6}\right)\frac{g^{i3}_{lq}\, g^{i2*}_{lq}}{M_U^2}, \tag{35}$$
$$[C_{dB}]_{23} = Y_b \frac{g'}{16\pi^2}\left(-\frac{4}{9}\right)\frac{g^{i2}_{lq}\, g^{i3*}_{lq}}{M_U^2},$$
$$[C_{dB}]_{32} = Y_s \frac{g'}{16\pi^2}\left(-\frac{4}{9}\right)\frac{g^{i3}_{lq}\, g^{i2*}_{lq}}{M_U^2}, \tag{36}$$

where Y_b and Y_s denote the Yukawa couplings of the b and s quark respectively and a summation over the lepton index is implied. The Wilson coefficients of the chromomagnetic dipole operators at the matching scale read

$$[C_{dG}]_{23} = Y_b \frac{g_s}{16\pi^2}\left(-\frac{5}{12}\right)\frac{g^{i2}_{lq}\, g^{i3*}_{lq}}{M_U^2},$$
$$[C_{dG}]_{32} = Y_s \frac{g_s}{16\pi^2}\left(-\frac{5}{12}\right)\frac{g^{i3}_{lq}\, g^{i2*}_{lq}}{M_U^2}. \tag{37}$$

Using the tree-level matching conditions from SMEFT onto WET [119,120], we have checked that these results are consistent with the findings in [98].

4.1.1 $R_{D^{(*)}}$ and indirect constraints

Within the defined framework we now search for a region of the leptoquark parameter space that explains all the B anomalies while at the same time avoids indirect low-energy constraints. We perform a fit with fixed $M_U = 2$ TeV in the space of tauonic couplings g^{32}_{lq} and g^{33}_{lq}, which we take to be real for simplicity. This allows us to determine the region in which $R_{D^{(*)}}$ can be explained by the semi-tauonic operators discussed in Sect. 3.3.1. The results of the fit are shown in Fig. 6 and our findings are as follows:

- The strongest constraints are due to
  - leptonic tau decays $\tau \to \ell\nu\nu$, which receive a contribution due to RG running,[13]

[13] Our analysis includes RG-induced logarithms. Note that the interactions in Eq. (29) and (33) provide a simplified model and not a complete UV theory of the U_1-leptoquark. In such a UV theory, it could in principle be possible that the RG-induced logarithms are (partially) canceled by finite terms, which are not present in the simplified model. See e.g. discussion in [118]. Barring cancellations, and in view of the renormalization-scale independence of the full result – logarithms plus analytic terms – the contributions from the RG-induced logarithms usually provide a realistic estimate of the size of the effects.

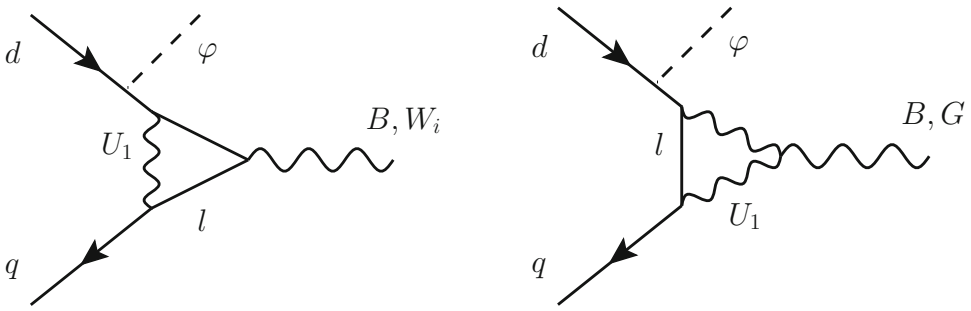

Fig. 5 Diagrams contributing to the matching of the U_1 leptoquark model onto the SMEFT operators O_{dB}, O_{dW} and O_{dG}

– BR($B \to X_s\gamma$), which receives a contribution from the one-loop matching onto dipole operators in SMEFT as discussed above.[14]

This underlines the importance of taking into account loop effects, both in the RG running and in the matching, as emphasized already in [98,122,123].

- A combined fit to $R_{D^{(*)}}$ and leptonic tau decays selects a well-defined region in the space of g_{lq}^{32} and g_{lq}^{33} in which $R_{D^{(*)}}$ can be explained while satisfying all constraints.
- In order to explain $R_{D^{(*)}}$ while at the same time avoiding exclusion at the 2σ level from leptonic tau decays, a minimal ratio of tauonic couplings $\frac{g_{lq}^{32}}{g_{lq}^{33}} \gtrsim 0.1$ is required (assuming vanishing right-handed couplings), which is compatible with findings in [113]. This puts some tension on models based on a $U(2)_q$ flavour symmetry [37,106,108,113], where the natural expectation for the size of $\frac{g_{lq}^{32}}{g_{lq}^{33}}$ is $|V_{cb}| \approx 0.04$.

Based on the above results, we select a benchmark point from the best-fit region in the fit to tauonic couplings,

$$g_{lq}^{32} = 0.6, \qquad g_{lq}^{33} = 0.7, \tag{38}$$

which is also shown in Fig. 6. We then perform two fits in the space of muonic couplings g_{lq}^{22} and g_{lq}^{23} shown in Fig. 7: one for vanishing tauonic couplings (left panel) and one at the benchmark point $g_{lq}^{32} = 0.6$, $g_{lq}^{33} = 0.7$ (right panel). Our findings are as follows:

- For vanishing tauonic couplings (left panel of Fig. 7), the data available before Moriond 2019 leads to a very good agreement between the fits to $b \to s\mu\mu$ (orange contour) and NCLFU observables (dashed blue contour), while the $R_{D^{(*)}}$ measurements cannot be explained in this scenario. Taking into account the updated and new measurements of $R_{K^{(*)}}$ presented at Moriond 2019, one finds a slight tension between the fits to $b \to s\mu\mu$ (orange contour) and NCLFU observables (solid blue contour). This is analogous to the tension mentioned in Sects. 3.1.2 and 3.1.3.
- The tension disappears if one considers non-zero tauonic couplings that can also explain $R_{D^{(*)}}$, which is exemplified in the right panel of Fig. 7 for the benchmark point $g_{lq}^{32} = 0.6$, $g_{lq}^{33} = 0.7$. As discussed in Sect. 3.2, the semi-tauonic operators obtained from the tree-level matching (cf. Eq. 30) induce a lepton-flavour universal contribution to C_9, which affects the predictions of $b \to s\mu\mu$ observables and makes the fits to $b \to s\mu\mu$ and NCLFU observables again compatible with each other at the 1σ level. Consequently, the deviations in neutral current and charged current B-decays can all be explained at once. This very well agrees with our findings in the SMEFT scenario in Sect. 3.3.1.

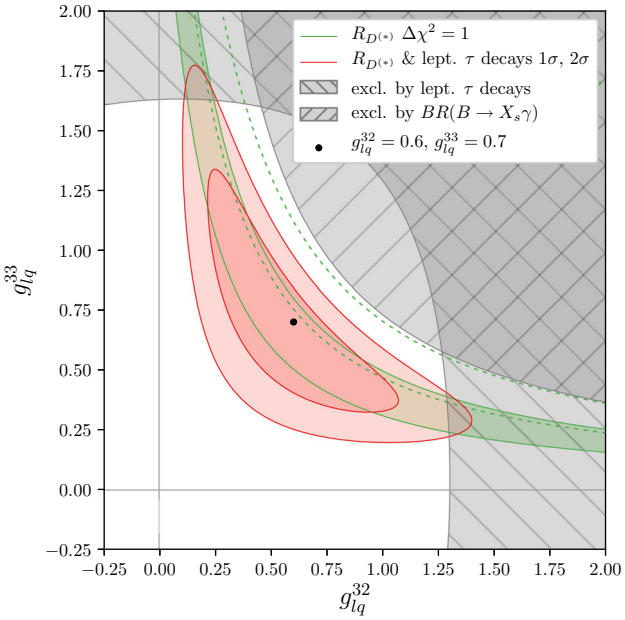

Fig. 6 Likelihood contours from different observables in the space of the tauonic U_1 leptoquark couplings g_{lq}^{32} and g_{lq}^{33} at 2 TeV. The grey areas are excluded at the 2σ level. $R_{D^{(*)}}$ data and leptonic τ decays select a well-defined region in the g_{lq}^{32} versus g_{lq}^{33} plane. For $R_{D^{(*)}}$, which only constrain one degree of freedom, 1σ contours correspond to $\Delta\chi^2 = 1$, while for others (the global likelihood, leptonic τ decays, BR($B \to X_s\gamma$)), 1 and 2σ contours correspond to $\Delta\chi^2 \approx 2.3$ and 6.2, respectively. The dashed contour refers to pre-Moriond data of the corresponding solid contour

[14] Such contributions are, however, model-dependent. For example, they will be quite different in models with additional vector-like fermions running in the loops [105,106], as shown explicitly in Ref. [121].

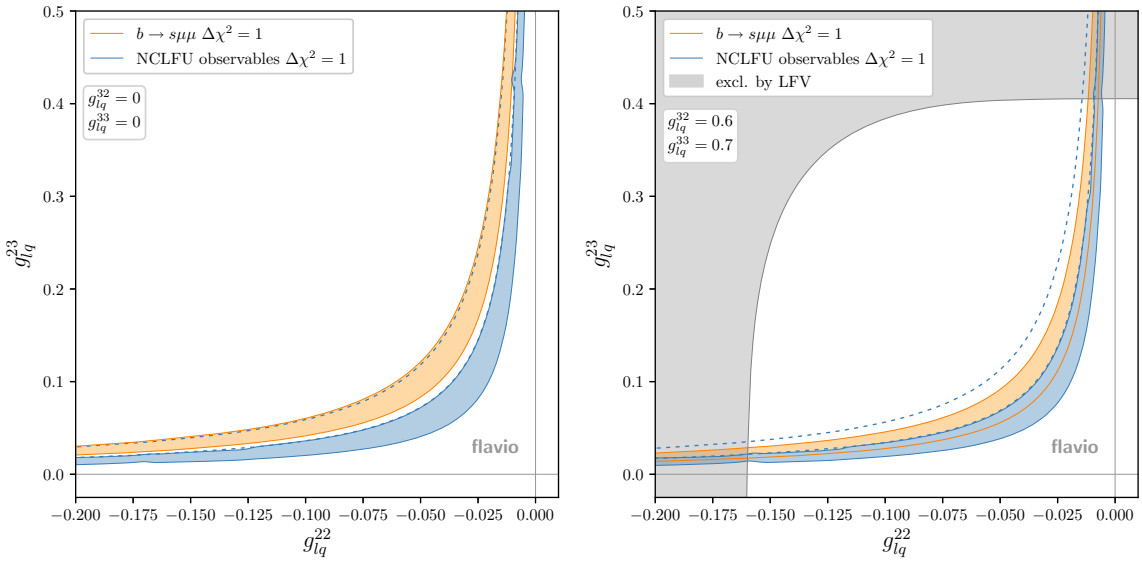

Fig. 7 Likelihood contours from different observables in the space of the muonic U_1 leptoquark couplings g_{lq}^{22} and g_{lq}^{23} at 2 TeV. Fits are shown for vanishing tauonic couplings $g_{lq}^{32} = 0$, $g_{lq}^{33} = 0$ (left) and at the benchmark point $g_{lq}^{32} = 0.6$, $g_{lq}^{33} = 0.7$ (right). The grey area is excluded at the 2σ level. For observables that only constrain one degree of freedom (here NCLFU and $b \to s\mu\mu$ observables), 1σ contours correspond to $\Delta\chi^2 = 1$, while for the lepton flavour violating observables, the 2σ contour corresponds to $\Delta\chi^2 \approx 6.2$. The dashed contours refer to pre-Moriond data of the corresponding solid contours

- Given the presence of non-zero values for the tauonic couplings at the benchmark point, the strongest constraint on the muonic couplings g_{lq}^{22} and g_{lq}^{23} is due to LFV observables, in particular $\tau \to \phi\mu$ and $B \to K\tau\mu$. The region in the space of muonic couplings that is excluded at the 2σ level by these observables is shown in gray in the right panel of Fig. 7.

Having identified a viable benchmark point, we conclude that the U_1 vector leptoquark can still provide an excellent description of the B anomalies while satisfying all indirect constraints.

4.1.2 Comparison between indirect and direct constraints

In addition to indirect constraints, high-p_T signatures of models containing a U_1 leptoquark have been discussed in detail considering current and future LHC searches [114, 124–128]. In this section, we compare direct constraints found in the latest study, [128], to the strong indirect constraints discussed in Sect. 4.1.1. To this end, we adopt the notation of [128] and use the parameters β_L^{ij} and g_U, which are related to our notation by

$$g_{lq}^{ij} = \frac{\beta_L^{ji}\, g_U}{\sqrt{2}}. \tag{39}$$

We perform a fit with fixed $g_U = 3$, $\beta_L^{33} = 1$ (i.e. $g_{lq}^{33} \approx 2$) in the space of M_U and β_L^{23}. These values are chosen to allow for a direct comparison with the constraint from $pp \to \tau\tau$ shown in Fig. 1 of [128] and $pp \to \tau\nu$ shown in Fig. 6 of [128]. We include both of these direct constraints in our Fig. 8 as hatched areas. In addition, we show the results from our fit, namely the constraint from leptonic τ decays and the region preferred by the $R_{D^{(*)}}$ measurements.

Our findings are as follows:

- The indirect constraint from leptonic τ decays is stronger than the direct constraints in nearly all of the parameter space shown in Fig. 8, except for a small region at large $\beta_L^{23} \gtrsim 0.75$, where the constraint from $pp \to \tau\nu$ is the strongest one.
- In the region where $R_{D^{(*)}}$ can be explained, the indirect constraint from leptonic τ decays is considerably stronger than the direct ones.
- Small values for $\frac{\beta_L^{23}}{\beta_L^{33}}$ as naturally expected in models based on a $U(2)_q$ flavour symmetry [37,106,108,113] require a relatively small mass M_U to explain $R_{D^{(*)}}$. Thus, as also pointed out in [113,124], there is already some tension between this natural expectation and the direct searches.

We note that the direct constraints shown in Fig. 8 depend on the coupling strength g_U. While the assumptions $g_U = 3$, $\beta_L^{33} = 1$ lead to a lower bound on the leptoquark mass $M_U \gtrsim 2.7$ TeV, this bound does not apply to the scenario discussed in

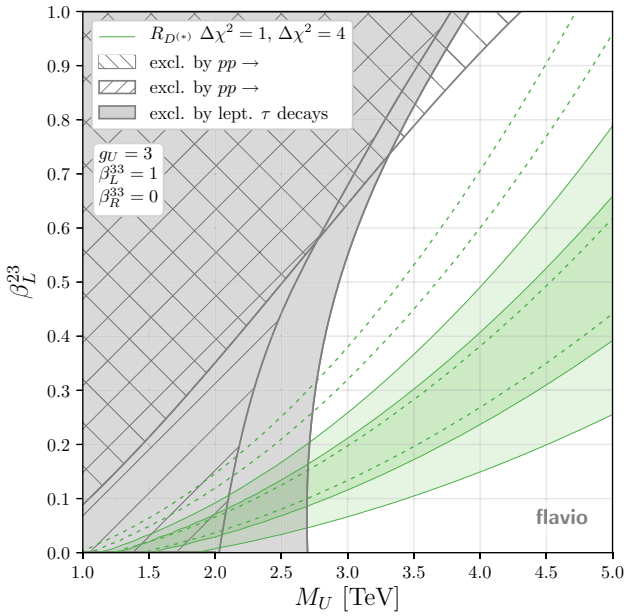

Fig. 8 Best fit region in the space of U_1 leptoquark mass M_U and coupling β_L^{23} (cf. Eq. (39)). The green region is the preferred region from $R_{D^{(*)}}$, while the gray shaded area is excluded by leptonic tau decays at the 2σ level. The hatched areas are excluded by LHC searches recasted in [128]

Sect. 4.1.1, which features considerably smaller couplings.[15] Latest direct constraints from U_1 pair production that are independent of the coupling strength g_U only exclude masses $M_U \lesssim 1.5$ TeV [114,128]. Therefore, the scenario discussed in Sect. 4.1.1 is currently not constrained by direct searches.

4.2 Lepton flavour universal C_9 from leptophobic mediators

As discussed in Sect. 3.3.2 in the SMEFT context, a lepton flavour universal contribution to C_9 can also be induced from a four-quark operator via RG effects. However, the four-quark operator would realistically have to be generated by the tree-level exchange of a resonance with mass not exceeding a few TeV and $O(1)$ couplings. Such resonance could then be in reach of direct LHC searches, apart from other indirect constraints.

Since it was shown in Sect. 3.3.2 that the only viable operators are of type $O_{qu}^{(1)}$ and $O_{qd}^{(1)}$, the conceivable tree-level mediators, excluding fields that admit baryon number violating diquark couplings,[16] are (see e.g. [129])

- $(\mathbf{1},\mathbf{1})_0$ with spin 1 (Z'),
- $(\mathbf{8},\mathbf{1})_0$ with spin 1 (G'),
- $(\mathbf{1},\mathbf{2})_{1/2}$ with spin 0 (H'),
- $(\mathbf{8},\mathbf{2})_{1/2}$ with spin 0 (Φ).

Such leptophobic mediators are discussed here mostly because they are a logical possibility – in particular, they are not necessarily motivated from a UV perspective. It is immediately clear that the spin-1 mediators Z' and G' are not viable: to generate the Wilson coefficients $[C_{qu}^{(1)}]_{23ii}$ or $[C_{qu}^{(1)}]_{23ii}$ with sufficient size, they would require a sizeable flavour-violating coupling to left-handed down-type quarks that would induce excessive contributions to B_s-$\bar{B}_s$ mixing. Thus the only potentially viable models are the scalar mediators.

The new scalar bosons have the following Lagrangian couplings to quarks,

$$\mathcal{L}_{H'} \supset y_{H'qu}^{ij}\, \bar{q}_i u_j \tilde{H}' - y_{H'qd}^{ij}\, \bar{q}_i d_j H' + \text{h.c.}, \tag{40}$$

$$\mathcal{L}_{\Phi} \supset y_{\Phi qu}^{ij}\, \bar{q}_i T^A u_j \tilde{\Phi}^A - y_{\Phi qd}^{ij}\, \bar{q}_i T^A d_j \Phi^A + \text{h.c.}\,. \tag{41}$$

The SMEFT Wilson coefficients that are generated by a tree-level scalar exchange and can contribute to C_9 via RG effects read

$$[C_{qR}^{(1)}]_{ijkl} = \sum_{X=H',\Phi} c_X \frac{y_{XqR}^{jk*} y_{XqR}^{il}}{M_X^2}, \tag{42}$$

where $R = u, d$ and $(c_{H'}, c_\Phi) = (-1/6, -2/9)$.

Clearly, to generate one of the down-type Wilson coefficients $[C_{qd}^{(1)}]_{23ii}$ in (28), at least one flavour-violating coupling in the down-aligned basis has to be present, leading to excessive contributions to B^0-$\bar{B}^0$ or B_s-$\bar{B}_s$ mixing. Thus we assume vanishing down-type couplings $y_{Xqd}^{ij} = 0$ in the following.

For the up-type couplings y_{Xqu}, it is instead convenient to work in the up-aligned basis (cf. footnote 10 for notation), as setting $\hat{y}_{Xqu}^{12} = \hat{y}_{Xqu}^{21} = 0$ allows avoiding dangerous contributions to D^0-$\bar{D}^0$ mixing. We then obtain the following non-vanishing matching conditions relevant for RG-induced contributions to C_9,

$$[C_{qu}^{(1)}]_{2311} = c_X \frac{1}{M_X^2} V_{is}^* V_{jb}\, \hat{y}_{Xqu}^{j1*} \hat{y}_{Xqu}^{i1} \approx c_X \frac{1}{M_X^2} \times \left(V_{us}^* V_{tb}\, \hat{y}_{Xqu}^{31*} \hat{y}_{Xqu}^{11} + V_{ts}^* V_{tb}\, |\hat{y}_{Xqu}^{31}|^2 + O(\lambda^3) \right), \tag{43}$$

$$[C_{qu}^{(1)}]_{2322} = c_X \frac{1}{M_X^2} V_{is}^* V_{jb}\, \hat{y}_{Xqu}^{j2*} \hat{y}_{Xqu}^{i2} \approx c_X \frac{1}{M_X^2} \left(V_{cs}^* V_{tb}\, \hat{y}_{Xqu}^{32*} \hat{y}_{Xqu}^{22} + V_{cs}^* V_{cb}\, |\hat{y}_{Xqu}^{22}|^2 + V_{ts}^* V_{tb}\, |\hat{y}_{Xqu}^{32}|^2 + O(\lambda^3) \right). \tag{44}$$

[15] The partonic cross section relevant for the direct constraints in Fig. 8 scales as $\sigma \sim (g_U/M_U)^4$ [128].

[16] Note that baryon number violating diquark couplings do not necessarily lead to tree-level proton decay.

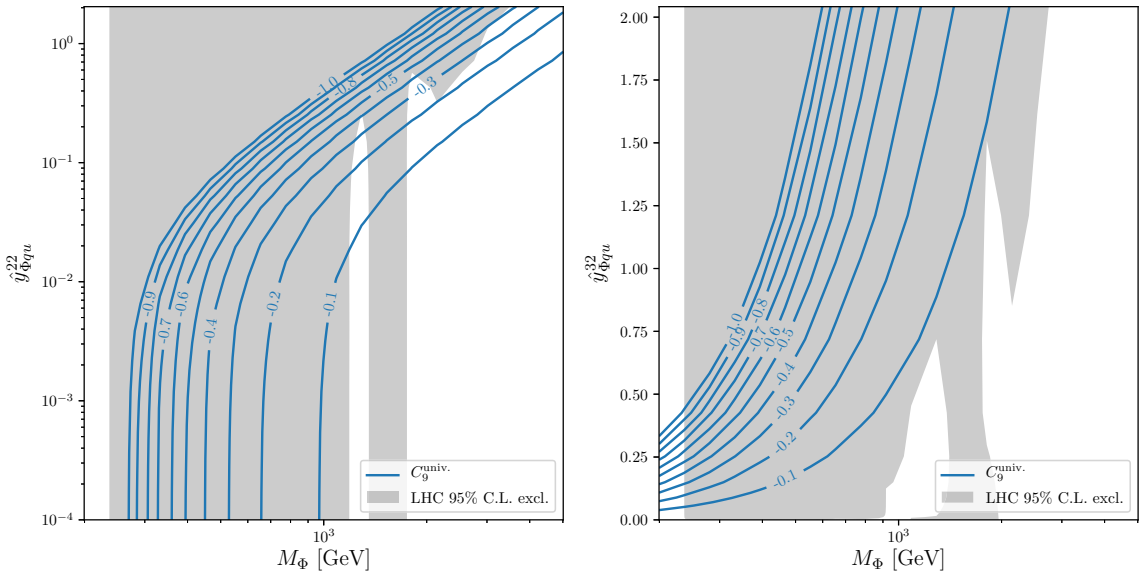

Fig. 9 Contours of constant $C_9^{\text{univ.}}$ in the colour octet scalar model vs. LHC di-jet exclusion for a scenario with $\hat{y}^{32}_{\Phi qu} = -1$ and varying $\hat{y}^{22}_{\Phi qu}$ (left) and for a scenario with $\hat{y}^{22}_{\Phi qu} = 0$ and varying $\hat{y}^{32}_{\Phi qu}$ (right)

Numerically, it turns out that a visible lepton flavour universal effect in C_9 requires $O(1)$ couplings for a scalar mass of the order of 2 TeV even for terms without CKM suppression. Thus, LHC searches for di-jet resonances are sensitive to the new scalars. If the NP effect in C_9 is generated through the terms in (43), the scalar has sizeable couplings to up quarks, leading to an excessive production cross section at the LHC. To avoid this, we will further assume $\hat{y}^{1i}_{Xqu} = \hat{y}^{i1}_{Xqu} = 0$ and use the terms in (44). Production in pp collisions is still possible via charm quarks. The leading-order cross sections of the charged and neutral components read

$$\sigma(pp \to X^\pm) = \tilde{c}_X \frac{\pi}{12s}\left[|\hat{y}^{22}_{Xqu}|^2\,(\mathcal{L}_{s\bar{c}} + \mathcal{L}_{c\bar{s}}) + |\hat{y}^{32}_{Xqu}|^2\,(\mathcal{L}_{b\bar{c}} + \mathcal{L}_{c\bar{b}})\right], \tag{45}$$

$$\sigma(pp \to X^0) = \tilde{c}_X \frac{\pi}{6s}|\hat{y}^{22}_{Xqu}|^2 \mathcal{L}_{c\bar{c}}, \tag{46}$$

where $(\tilde{c}_{H'}, \tilde{c}_\Phi) = (1, 4/3)$, $\sqrt{s}$ being the center of mass energy and $\mathcal{L}_{ij}$ are the parton luminosities as defined in [130] and we have neglected contributions suppressed by CKM factors.

We confront these cross sections with exclusion limits from ATLAS [131] and CMS [132]. Our procedure to obtain constraints on the scalar model parameters is detailed in Appendix D. For definiteness, we choose $X = \Phi$ in the following. In fact, according to the results of [99], the H' case is considerably more constrained by contributions to $B \to X_s\gamma$ introduced radiatively at the two-loop level.

The left plot in Fig. 9 shows contours of $C_9^{\text{univ.}}$ in the plane of $\hat{y}^{22}_{\Phi qu}$ vs. the color-octet scalar mass for a scenario in which $\hat{y}^{32}_{\Phi qu} = -1$. We also show the 95% C.L. exclusion from di-jet resonance searches at LHC. Obviously, a visible negative contribution to $C_9^{\text{univ.}}$ of at most -0.3 can only be generated in a thin sliver of parameter space for masses above 2 TeV and with $\hat{y}^{22}_{\Phi qu} \sim 1$. This scenario is on the brink of exclusion.[17] The bending of the $C_9^{\text{univ.}}$ contours at low masses in the left plot of Fig. 9 is due to the fact that there is a CKM-suppressed contribution even for $\hat{y}^{22}_{\Phi qu} = 0$ from the third term in (44). To investigate whether such scenario, where production is only possible through a b quark PDF, is allowed, in the right plot of Fig. 9 we show the $C_9^{\text{univ.}}$ contours and the LHC exclusion for $\hat{y}^{32}_{\Phi qu}$ vs. the color octet scalar mass setting $\hat{y}^{22}_{\Phi qu} = 0$. Clearly, generating an appreciable contribution to $C_9^{\text{univ.}}$ is excluded by di-jet searches in this scenario.

5 Conclusions

Motivated by the updated measurements of the theoretically clean lepton flavour universality tests R_K and R_{K^*} by the LHCb and Belle experiments, as well as by additional measurements, notably of $B_s \to \mu\mu$ by the ATLAS collaboration, we have updated the global EFT analysis of new physics in $b \to s\ell\ell$ transitions. A new-physics effect in the semi-muonic Wilson coefficient $C_9^{bs\mu\mu}$ continues to give a much improved fit to the data compared to the SM. However, compared to previous global analyses, we find that there is now

[17] If one allows for enlarged hadronic uncertainties (see discussion end of Sect. 3.1.3), the parameter space that is not yet excluded by LHC searches can open up slightly.

also a preference for a non-zero value of the semi-muonic Wilson coefficient $C_{10}^{bs\mu\mu}$, mostly driven by the global combination of the $B_s \to \mu^+\mu^-$ branching ratio including the ATLAS measurement. The single-coefficient scenario giving the best fit to the data is the one where $C_9^{bs\mu\mu} = -C_{10}^{bs\mu\mu}$, which is known to be well suited to UV-complete interpretations, and indeed is predicted in several new-physics models with tree-level mediators coupling dominantly to left-handed fermions.

We have also studied the possibility of a simultaneous interpretation of the $b \to s\ell\ell$ data and the discrepancies in $b \to c\tau\nu$ transitions in the framework of a global likelihood in SMEFT Wilson coefficient space. We find one especially compelling scenario, characterised by new physics in all-left-handed semitauonic four-fermion operators. These operators can explain directly the discrepancies in $b \to c\tau\nu$ transitions, and, at the same time, radiatively induce a lepton flavour universal contribution to the $b \to s\ell\ell$ Wilson coefficients. An additional nonzero semimuonic Wilson coefficient then allows accommodating the $R_{K^{(*)}}$ discrepancies. Such picture can be quantitatively realized in the context of the U_1 leptoquark simplified model, and we find that indeed an excellent description of the data can be obtained, including the deviations in $b \to c\tau\nu$ transitions.

Another logical possibility to generate a lepton flavour universal NP effect in C_9 is via RG effects from a four-quark operator. We have investigated this possibility in the SMEFT and in simplified tree-level models. We find that the only setup potentially viable in the light of indirect constraints is a colour-octet scalar. However, due to its TeV-scale mass and large coupling to quarks, it is strongly constrained by di-jet resonance searches at the LHC, which put it on the brink of exclusion.

Our study illustrates how the theoretical picture has evolved as a consequence of crucial measurement updates, and how this picture stays coherent in spite of the numerous constraints. We collect in Table 2 a number of predictions directly related to the discussed SMEFT scenario. The situation will only get more exciting due to the host of new analyses using the full Run-2 data set, as well as the Belle-II data set, to which we look forward.

Acknowledgements D.S. warmly thanks the organisers of the Rencontres de Moriond 2019 on "Electroweak Interactions and Unified Theories" for the opportunity to present the results in this paper prior to their appearance on the arXiv. We also acknowledge useful remarks from Ben Allanach and Sébastien Descotes-Genon. The work of D. S. and J. A. is supported by the DFG cluster of excellence "Origin and Structure of the Universe". The research of W. A. is supported by the National Science Foundation under Grant No. NSF 1912719. The numerical analysis has been carried out on the computing facilities of the Munich Computational Center for Particle and Astrophysics (C2PAP).

Data Availability Statement This manuscript has no associated data or the data will not be deposited. [Authors' comment: This is a theoretical study, with no experimental data generated.]

Funded by SCOAP[3].

A Combination of $B_q \to \mu^+\mu^-$ measurements

In this appendix we discuss our procedure of combining the measurements by ATLAS, CMS, and LHCb of the branching ratios of $B^0 \to \mu^+\mu^-$ and $B_s \to \mu^+\mu^-$ [46–49].

In all three cases, the measurements are correlated, since the B^0 and B_s have a similar mass, such that the signal regions in dimuon invariant mass squared overlap. ATLAS and CMS provide two-dimensional likelihood contours, from which we interpolate the two-dimensional likelihoods, while LHCb directly provides the two-dimensional likelihood numerically. The three resulting likelihoods are shown as thin lines in Fig. 10 and compared to the SM central values.

Next, we assume the three experiments to be uncorrelated (which we assume to be a good approximation given the dominance of statistical uncertainties) and combine the two-

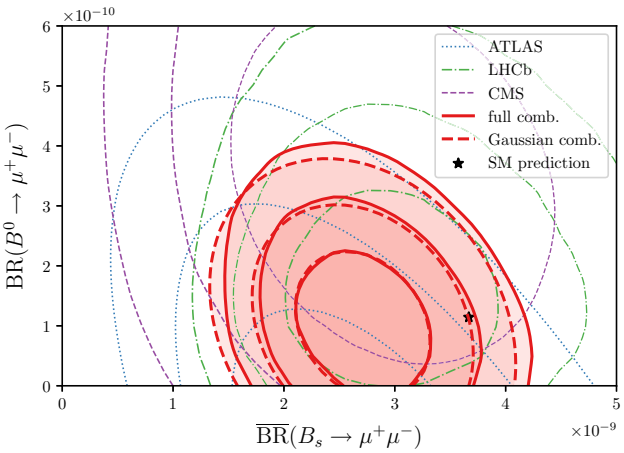

Fig. 10 Two-dimensional likelihood contours in the space of the $B^0 \to \mu^+\mu^-$ and $B_s \to \mu^+\mu^-$ branching ratios from individual measurements (thin contours), the naive combination (thick solid contours), and the Gaussian approximation to it (thick dashed contours), compared to the SM central values

dimensional likelihoods by multiplying them. The resulting contour is also shown in Fig. 10.

For our global likelihood in Wilson coefficient space, we need to make an additional approximation, namely that the experimental likelihood is approximately Gaussian (see [53] for a discussion). Thus we fit a two-dimensional Gaussian to the product likelihood. The resulting contours are shown as thick dashed lines in Fig. 10.

Since throughout our numerical analysis, we never consider NP effects in $b \to d\mu\mu$ transitions, it is also interesting to compare the combined confidence regions for the $B_s \to \mu^+\mu^-$ branching ratio, fixing $B^0 \to \mu^+\mu^-$ to its SM central value or profiling over it. We find

$$\overline{\text{BR}}(B_s \to \mu^+\mu^-) = (2.67^{+0.45}_{-0.35}) \times 10^{-9} \quad \text{BR}(B^0 \to \mu^+\mu^-) \text{ profiled}, \tag{47}$$

$$\overline{\text{BR}}(B_s \to \mu^+\mu^-) = (2.65^{+0.46}_{-0.33}) \times 10^{-9} \quad \text{BR}(B^0 \to \mu^+\mu^-) \text{ SM-like}. \tag{48}$$

We stress that the similarity of these two numbers is not trivial, as for individual measurements, especially the CMS and ATLAS ones, the best-fit value for $\text{BR}(B^0 \to \mu^+\mu^-)$ deviates strongly from the SM prediction. Conversely, for $B^0 \to \mu^+\mu^-$ we get

$$\text{BR}(B^0 \to \mu^+\mu^-) = (1.00^{+0.86}_{-0.57}) \times 10^{-10} \quad \overline{\text{BR}}(B_s \to \mu^+\mu^-) \text{ profiled}, \tag{49}$$

$$\text{BR}(B^0 \to \mu^+\mu^-) = (0.57^{+0.86}_{-0.36}) \times 10^{-10} \quad \overline{\text{BR}}(B_s \to \mu^+\mu^-) \text{ SM-like}. \tag{50}$$

The values for the Gaussian approximation only differ from these numbers in a negligible way.

Compared to the SM predictions[18]:

$$\overline{\text{BR}}(B_s \to \mu^+\mu^-)_{\text{SM}} = (3.67 \pm 0.15) \times 10^{-9}, \tag{51}$$

$$\text{BR}(B^0 \to \mu^+\mu^-)_{\text{SM}} = (1.14 \pm 0.12) \times 10^{-10}, \tag{52}$$

we then find the following one-dimensional pulls:[19]

- if both branching ratios are SM-like, 2.3σ,[20]
- if $B_s \to \mu^+\mu^-$ is SM-like and $B^0 \to \mu^+\mu^-$ profiled over, 2.3σ,
- if $B^0 \to \mu^+\mu^-$ is SM-like and $B_s \to \mu^+\mu^-$ profiled over, 0.2σ.

[18] For the SM values, we have used `flavio` v1.3 with default settings. The $B_s \to \mu^+\mu^-$ branching ratio refers to the time-integrated one, see Refs. [133,134] for state-of-the-art discussions on the SM uncertainty. The decay constants are taken from the 2019 FLAG average with $2+1+1$ flavours [135], $V_{cb} = 0.04221(78)$ from inclusive decays, and $V_{ub} = 0.00373(14)$ from $B \to \pi\ell\nu$.

[19] Here, the "one-dimensional pull" is -2 times the logarithm of the likelihood ratio at the SM vs. the experimental point, after the experimental uncertainties have been convolved with the covariance of the SM uncertainties.

[20] Converting the likelihood ratio to a pull with two degrees of freedom, one obtains 1.8σ; this is why the star in Fig. 10 is inside the 2σ contour.

B. Global likelihood of the standard model

In view of the sizable pulls in various NP scenarios considered in this work, an interesting question is how good the overall agreement of the SM with the data is. To this end, we consider the value of the global likelihood at the SM point, $L(\vec{0})$, or $\chi^2_{\text{SM}} \equiv -2\ln L(\vec{0})$. Here, the normalization of the likelihood is such that $\chi^2 = 0$ corresponds to the case where all measurements are in exact agreement with the theoretical predictions. By means of Wilks' theorem, this χ^2 value can be translated to a p-value, quantifying the goodness of fit.

However, the intepretation of this global χ^2 value is not straightforward as it is subject to several ambuguities.

- Since the global likelihood contains many observables not sensitive to the Wilson coefficients that we consider in our analysis, which focuses on discrepancies in B physics, this p-value depends on the number of observables included in the test.
- The likelihood contains measurements that are actually averages (e.g. by PDG or HFLAV) of several measurements, such that the number of degrees of freedom is reduced and a constant contribution to the χ^2 coming from a tension between the averaged measurements is concealed.
- Due to the statistical approach, where theory uncertainties are combined with the experimental ones and no explicit nuisance parameters are present, the contribution to the absolute χ^2 from different sectors can depend sensitively on the central values chosen for the parameters. For instance, a lower V_{cb} value would lead to better agreement of $b \to s\ell\ell$ branching ratios (via lower $|V_{tb}V_{ts}^*|$) but worse agreement with $b \to c\ell\nu$ transitions. While this issue does not affect the $\Delta\chi^2$ used in our numerical analysis, it makes the interpretation of the absolute χ^2 for individual sectors difficult.

With these caveats in mind, we provide in Table 3 the absolute χ^2 values obtained with `smelli` for various subsets of observables. The number N_{obs} in the first column refers to the number of *observations*, i.e. independent measurements of an observable, which is greater than or equal to the number of *observables*. In our case, N_{obs} is to be interpreted as the χ^2's number of degrees of freedom. Through the `chi2_dict` method introduced in v1.3, it is possible to explore the χ^2 also for different observable sets or parameter inputs.

Table 3 Absolute χ^2 values and p-values for the global fit and various subsets of observables

Observables	N_{obs}	χ^2	p-value [%]
$b \to s\ell\ell$	127	126.7	49
$+R_{K^{(*)}} + D^{\mu e}_{P_i'}$	138	149.9	23
$+B_s \to \mu^+\mu^- + b \to s\gamma$	143	155.9	22
$+\Delta F = 2$	149	193.4	0.8
$+b \to c\tau\nu$	218	264.7	1.7
All quark flavour	258	301.9	3.1
All low-energy	276	308.6	8.6
Global	313	361.4	3.1

C. C_9 vs. $C_9 = -C_{10}$

As already discussed in Sect. 3.1.1 and summarized in Table 1, we find a preference for the $C_9^{bs\mu\mu} = -C_{10}^{bs\mu\mu}$ scenario over the $C_9^{bs\mu\mu}$-only scenario. Since the opposite result was found in previous analyses, like e.g. [29], some further comments are in order. The change in preference is not related to the updated measurements of R_K and R_{K^*} but can be traced back to the inclusion of several observables into the likelihood that were not considered in [29].[21] Among the newly included observables mentioned in Sect. 2, the following are in particular relevant here.

- The new ATLAS measurement of $\text{BR}(B_{s,d} \to \mu^+\mu^-)$ [46], which we combine with the measurements by LHCb and CMS [47–49] using the procedure detailed in Appendix A.
- The LHCb measurements of $\Lambda_b \to \Lambda\ell^+\ell^-$ observables [60].
- $\Delta F = 2$ observables,[22] most importantly ε_K and ΔM_s. Like the theoretical predictions for $\text{BR}(B_{s,d} \to \mu^+\mu^-)$, also the predictions for these observables depend on the $B_{s,d}$-meson decay constants $F_{B_{s,d}}$ and the CKM parameters. As detailed in [53], these nuisance parameters are "integrated out" and enter the likelihood in terms of a covariance matrix that contains all experimental and theoretical uncertainties together with their correlations. Due to these correlations, experimental information on $\Delta F = 2$ observables can reduce the theoretical uncertainties of $\text{BR}(B_{s,d} \to \mu^+\mu^-)$. Such a reduction of the theoretical uncertainties has been discussed explicitly for $\Delta M_{s,d}$ and $\text{BR}(B_{s,d} \to \mu^+\mu^-)$ in models with minimal flavour violation in [140]. Via the correlations, $\Delta F = 2$ observables can have an impact on a fit to the Wilson coefficients $C_9^{bs\mu\mu}$ and $C_{10}^{bs\mu\mu}$ even if they do not directly depend on these coefficients themselves.

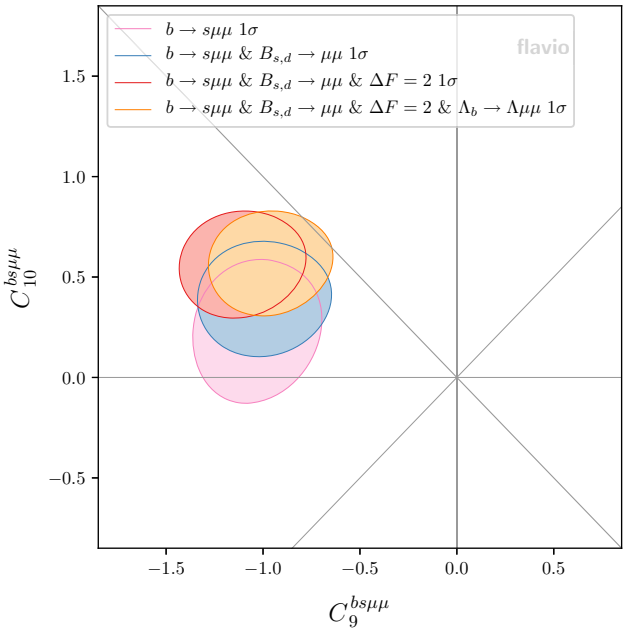

Fig. 11 The 1σ contour for the $b \to s\mu\mu$ likelihood, as a function of the observables detailed in the legend. The last contour in the legend, displayed in yellow, coincides with the corresponding one in Fig. 1 (left)

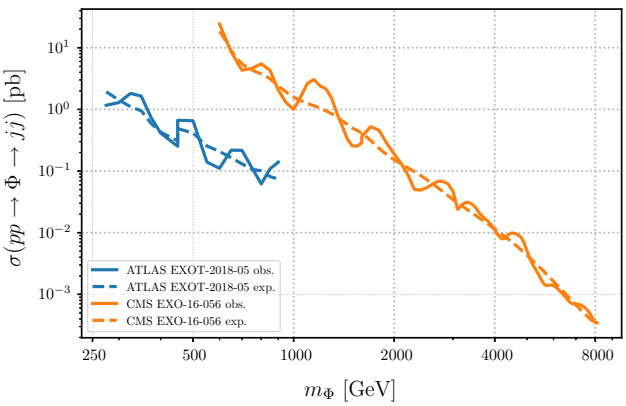

Fig. 12 95% C.L. observed and expected limits on the di-jet cross section in 13 TeV pp collisions from the two analyses used in Sect. 4.2. For the assumptions on efficiencies and acceptances see main text

To illustrate the effect of including the above listed observables into the likelihood, we show 1σ contours for several fits to subsets of observables in Fig. 11.

- The pink contour corresponds to a fit including only $b \to s\mu\mu$ observables excluding $\text{BR}(B_{s,d} \to \mu^+\mu^-)$. This fit is equivalent to the one shown in [29] and clearly prefers the $C_9^{bs\mu\mu}$-only scenario over the $C_9^{bs\mu\mu} = -C_{10}^{bs\mu\mu}$ one.

[21] Also other post-Moriond 2019 global fits that appeared slightly before and after the preprint of this paper use different sets of observables and found a preference for the $C_9^{bs\mu\mu}$-only scenario [97,136–139].

[22] For the full list of observables, see [53].

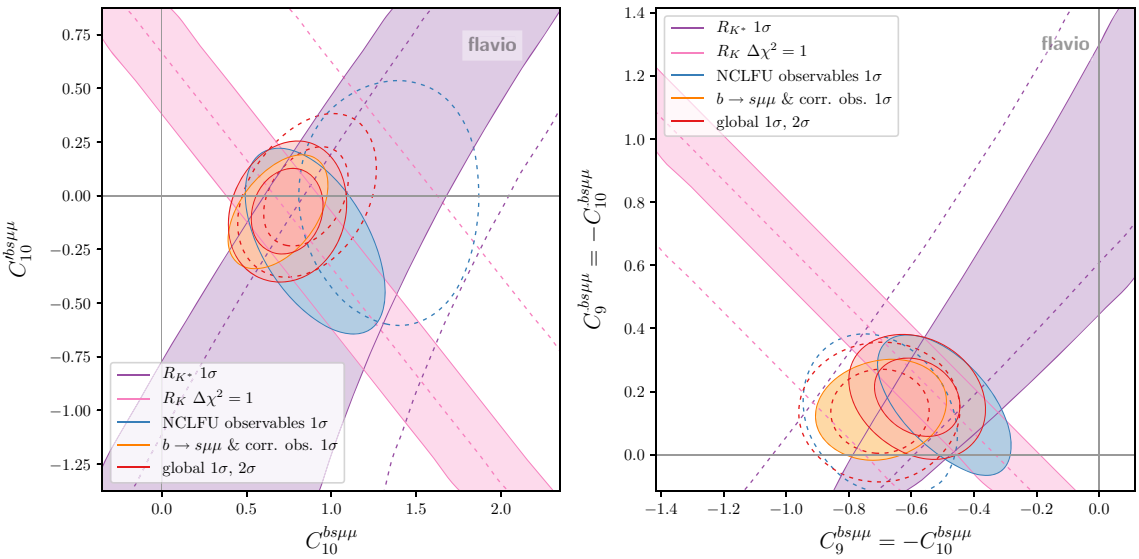

Fig. 13 Likelihood contours from NCLFU observables ($R_{K^{(*)}}$ and $D_{P'_{4,5}}$), $b \to s\mu\mu$ observables and the global likelihood in the space of $C_{10}^{bs\mu\mu}$ and $C_{10}^{\prime bs\mu\mu}$ (left) and in the space of $C_9^{bs\mu\mu} = -C_{10}^{bs\mu\mu}$ and $C_9^{\prime bs\mu\mu} = -C_{10}^{\prime bs\mu\mu}$ (right). All other Wilson coefficients are assumed to vanish. Solid (dashed) contours include (exclude) the Moriond-2019 results for R_K and R_{K^*}

- The blue contour is obtained from a fit that also includes $\mathrm{BR}(B_{s,d} \to \mu^+\mu^-)$. Due to the slight tension between experimental data and SM prediction of $\overline{\mathrm{BR}}(B_s \to \mu^+\mu^-)$ (cf. App. A), a non-zero NP contribution to $C_{10}^{bs\mu\mu}$ is preferred. In this case, the $C_9^{bs\mu\mu}$-only scenario and the $C_9^{bs\mu\mu} = -C_{10}^{bs\mu\mu}$ scenario perform similarly well and neither of them is clearly preferred.
- The red contour corresponds to a fit that additionally includes $\Delta F = 2$ observables. As described above, taking them into account can have an effect on the uncertainties of $B_s \to \mu\mu$ and we find that this leads to an increased preference for a non-zero NP contribution to $C_{10}^{bs\mu\mu}$. In this case, $C_9^{bs\mu\mu} = -C_{10}^{bs\mu\mu}$ is favoured over $C_9^{bs\mu\mu}$-only.
- The orange contour is obtained by adding $\Lambda_b \to \Lambda\ell^+\ell^-$ observables to the fit. While this does not further increase the preference for a non-zero NP contribution to $C_{10}^{bs\mu\mu}$, this contour now intersects with the $C_9^{bs\mu\mu} = -C_{10}^{bs\mu\mu}$ line, making this scenario clearly preferred over the $C_9^{bs\mu\mu}$-only one.

Other observables that are correlated with the $b \to s\mu\mu$ observables (e.g. $b \to s\gamma$) only have a marginal impact on the fit. Therefore, the orange contour in Fig. 11 essentially coincides with the orange contour in Fig. 1 left.

Note that the main effect of the correlations between the $C_{10}^{bs\mu\mu}$-dependent observables and the $\Delta F = 2$ observables vanishes if the theory predictions of the $\Delta F = 2$ observables exactly equal the corresponding experimental values. This means that neglecting the effect of the correlated $\Delta F = 2$ observables is equivalent to assuming NP contributions that shift all of them exactly to the experimentally measured values. Rather than relying on such a strong hypothesis, we

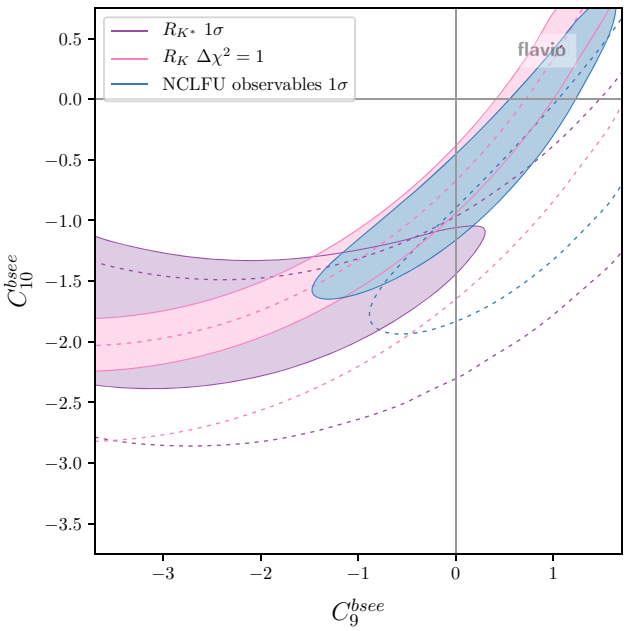

Fig. 14 Likelihood contours from NCLFU observables ($R_{K^{(*)}}$ and $D_{P'_{4,5}}$) in the space of C_9^{bsee} and C_{10}^{bsee}. All other Wilson coefficients are assumed to vanish. Solid (dashed) contours include (exclude) the Moriond-2019 results for R_K and R_{K^*}

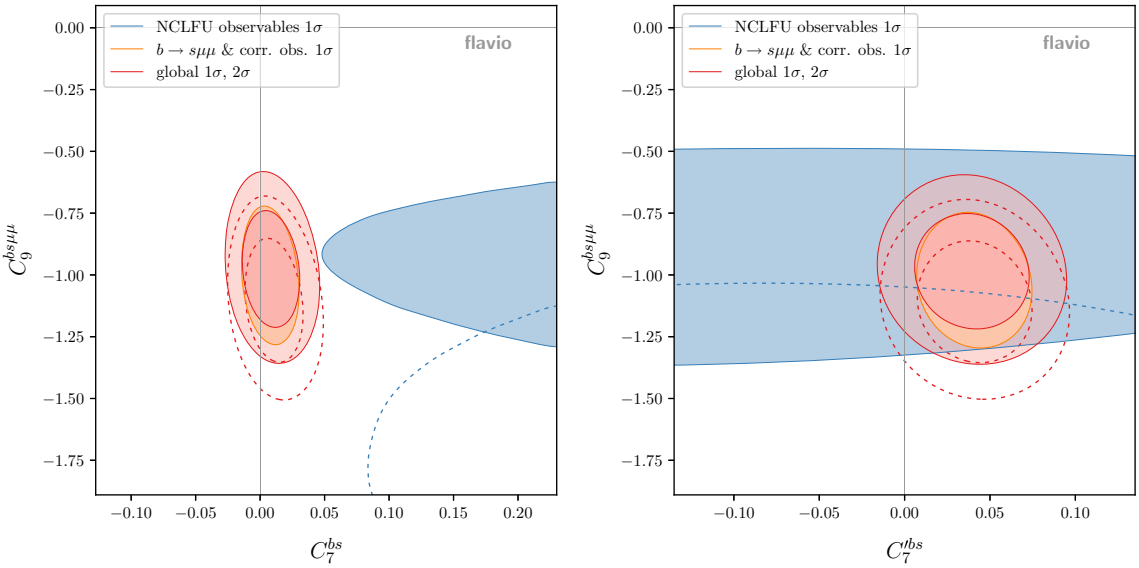

Fig. 15 Likelihood contours from NCLFU observables ($R_{K^{(*)}}$ and $D_{P'_{4,5}}$), $b \to s\mu\mu$ observables and the global likelihood in the space of C_7^{bs} and $C_9^{bs\mu\mu}$ (left) and in the space of C'^{bs}_7 and $C_9^{bs\mu\mu}$ (right). All other Wilson coefficients are assumed to vanish. Solid (dashed) contours include (exclude) the Moriond-2019 results for R_K and R_{K^*}

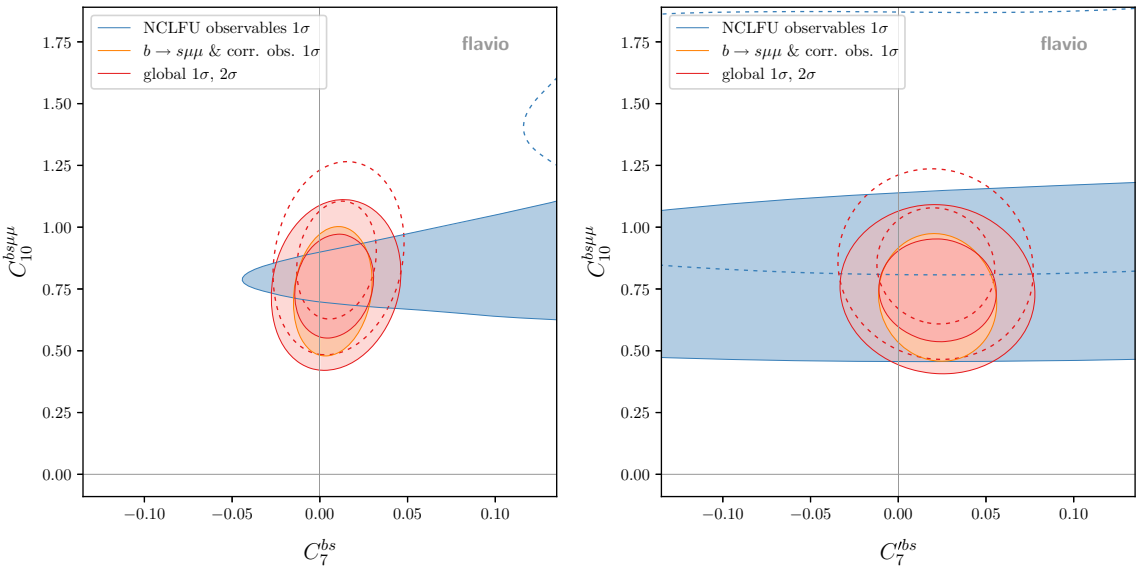

Fig. 16 Likelihood contours from NCLFU observables ($R_{K^{(*)}}$ and $D_{P'_{4,5}}$), $b \to s\mu\mu$ observables and the global likelihood in the space of C_7^{bs} and $C_{10}^{bs\mu\mu}$ (left) and in the space of C'^{bs}_7 and $C_{10}^{bs\mu\mu}$ (right). All other Wilson coefficients are assumed to vanish. Solid (dashed) contours include (exclude) the Moriond-2019 results for R_K and R_{K^*}

assume the theory predictions of $\Delta F = 2$ observables to be SM-like.[23]

[23] Many NP models that explain the deviations in rare B decays also predict a NP contribution to the Wilson coefficient C_{VLL}^{bsbs} of the operator $(\bar{s}_L\gamma^\mu b_L)\,(\bar{s}_L\gamma^\mu b_L)$, which modifies the theory prediction of ΔM_s. A large class of models predicts $\Delta M_s > \Delta M_s^{\rm SM}$ [141–143]. We have explicitly checked that a contribution to C_{VLL}^{bsbs} that increases ΔM_s up to its 2σ experimental bound can only marginally decrease the preference for a non-zero $C_{10}^{bs\mu\mu}$. On the other hand, any model that predicts $\Delta M_s < \Delta M_s^{\rm SM}$ would further increase this preference. Assuming SM-like theory predictions for $\Delta F = 2$ observables, the dominant effect of the correlations is due to ε_K.

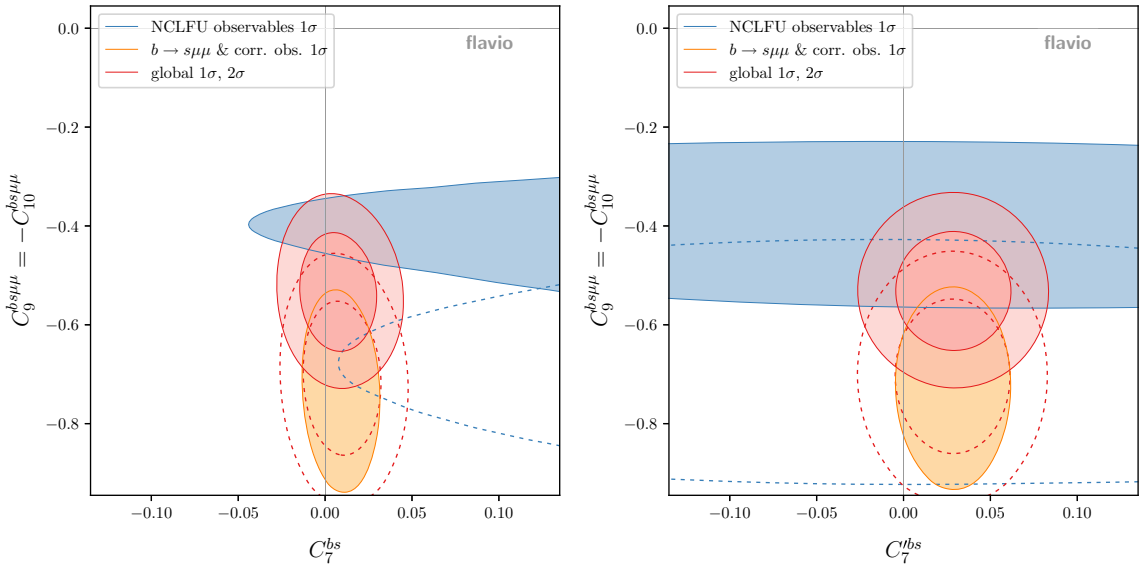

Fig. 17 Likelihood contours from NCLFU observables ($R_{K^{(*)}}$ and $D_{P'_{4,5}}$), $b \to s\mu\mu$ observables and the global likelihood in the space of C_7^{bs} and $C_9^{bs\mu\mu} = -C_{10}^{bs\mu\mu}$ (left) and in the space of $C_7'^{bs}$ and $C_9^{bs\mu\mu} = -C_{10}^{bs\mu\mu}$ (right). All other Wilson coefficients are assumed to vanish. Solid (dashed) contours include (exclude) the Moriond-2019 results for R_K and R_{K^*}

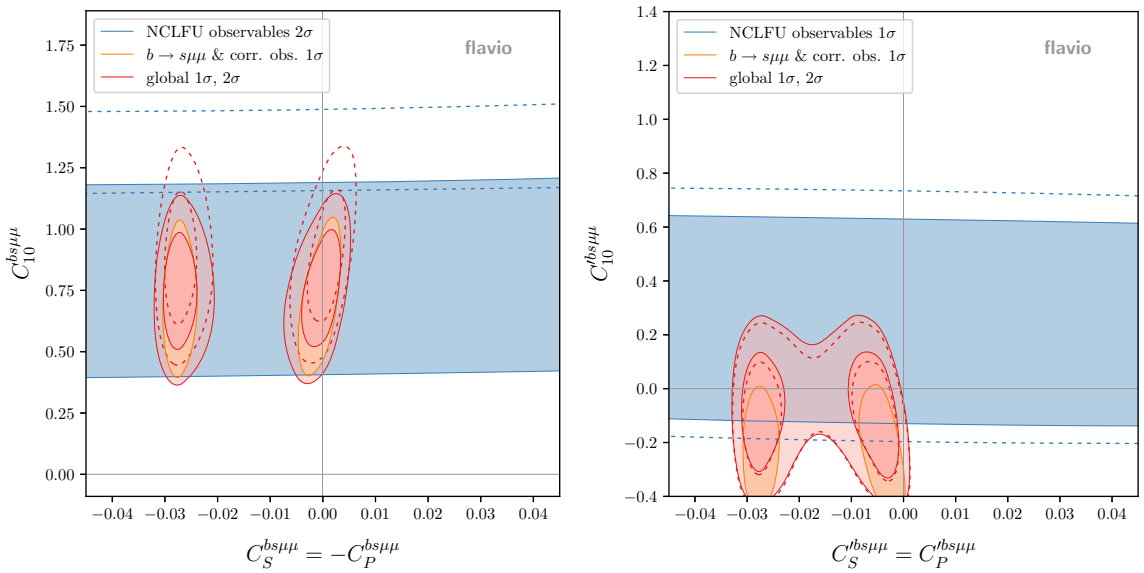

Fig. 18 Likelihood contours from NCLFU observables ($R_{K^{(*)}}$ and $D_{P'_{4,5}}$), $b \to s\mu\mu$ observables and the global likelihood in the space of $C_S^{bs\mu\mu} = -C_P^{bs\mu\mu}$ and $C_{10}^{bs\mu\mu}$ (left) and in the space of $C_S'^{bs\mu\mu} = C_P'^{bs\mu\mu}$ and $C_{10}'^{bs\mu\mu}$ (right). All other Wilson coefficients are assumed to vanish. Solid (dashed) contours include (exclude) the Moriond-2019 results for R_K and R_{K^*}

D. Di-jet bounds on leptophobic mediators

As discussed in Sect. 4.2, generating a LFU contribution to C_9 radiatively from four-quark operators requires a fairly light scalar mediator with strong coupling to quarks, that can lead to a signal in di-jet resonance searches at the LHC. In our numerical analysis, we employ two recent di-jet resonance searches.

- A search at $\sqrt{s} = 13$ TeV by CMS based on 36 fb^{-1} and covering the mass range from 600 to 8100 GeV [132]. We apply the 95% C.L. constraint on the production cross section times branching ratio times acceptance, assuming

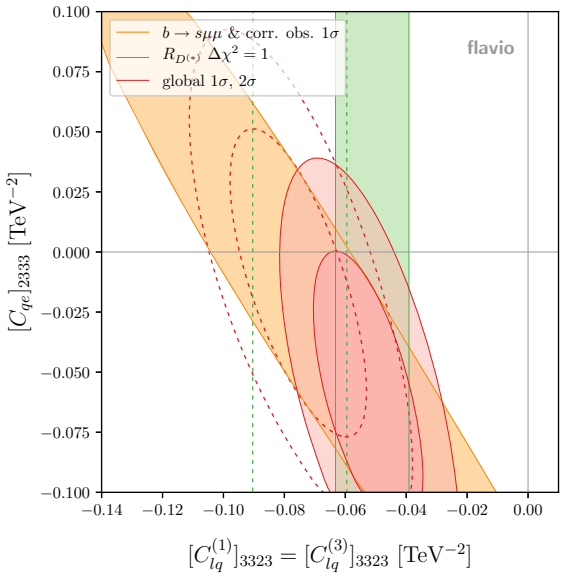

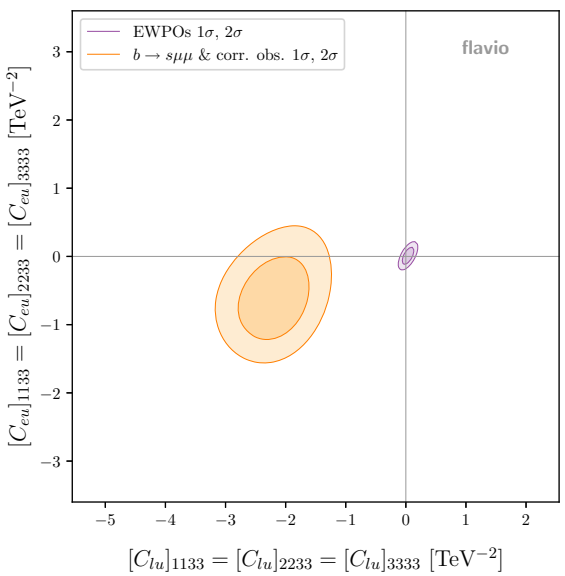

Fig. 19 Likelihood contours from $R_{D^{(*)}}$, $b \to s\mu\mu$ observables and the global likelihood in the space of $[C_{lq}^{(1)}]_{3323} = [C_{lq}^{(3)}]_{3323}$ and $[C_{qe}]_{2333}$ (left) and in the space of $[C_{lu}]_{1133} = [C_{lu}]_{2233} = [C_{lu}]_{3333}$ and $[C_{eu}]_{1133} = [C_{eu}]_{2233} = [C_{eu}]_{3333}$ (right) at 2 TeV. All other Wilson coefficients are assumed to vanish at 2 TeV

100% decay into di-jets and a constant acceptance of 57%.

- A search at $\sqrt{s} = 13$ TeV by ATLAS based on 80 fb^{-1} employing initial state radiation to cover the low-mass range not covered by CMS [131]. We apply the 95% C.L. constraint on the production cross section times branching ratio times acceptance times efficiency, assuming 100% decay into di-jets and using the mass-dependent efficiency and acceptance for the Z' model given in the publication.

The 95% C.L. bounds under these assumptions are shown in Fig. 12.

E. WET and SMEFT scenarios with Wilson coefficient pairs

The aim of this appendix is to present additional projections of the likelihood onto pairs of Wilson coefficients both in WET and SMEFT.

- The plots of Fig. 13 complement the ones in Fig. 1 and show Wilson coefficient spaces involving muonic axial-vector currents $C_{10}^{bs\mu\mu}$ and $C_{10}^{\prime bs\mu\mu}$.
- Fig. 14 shows the space of electronic Wilson coefficients C_9^{bsee} and C_{10}^{bsee}. R_K and R_{K^*} can be explained simultaneously if both C_9^{bsee} and C_{10}^{bsee} are present.
- The plots in Figs. 15, 16, and 17 explore the impact of non-standard effects in the dipole coefficients C_7^{bs} and $C_7^{\prime bs}$ that are switched on in addition to new physics in $C_9^{bs\mu\mu}$ (Fig. 15), $C_{10}^{bs\mu\mu}$ (Fig. 16), and $C_9^{bs\mu\mu} = -C_{10}^{bs\mu\mu}$ (Fig. 17). The fits prefer C_7^{bs} to be SM-like but show a slight ($\sim 1\sigma$) preference for a positive shift in $C_7^{\prime bs}$.
- In Fig. 18 we consider the effects of non-zero scalar and pseudo-scalar Wilson coefficients that obey the SMEFT

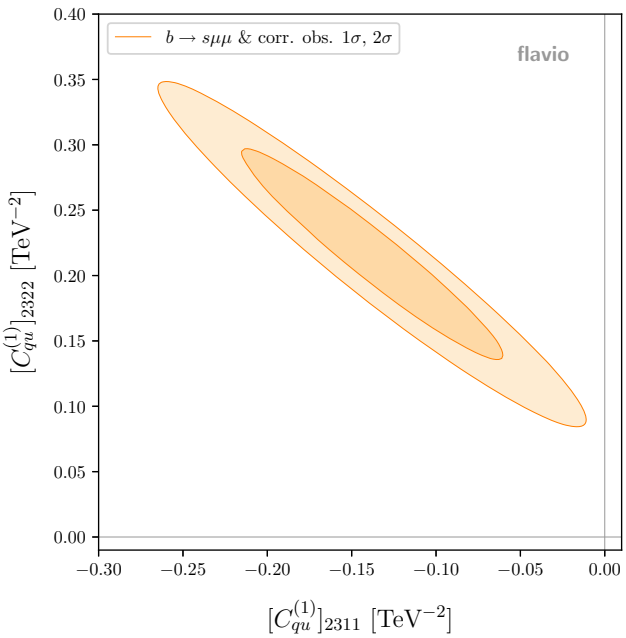

Fig. 20 Likelihood contours from $b \to s\mu\mu$ observables in the space of $[C_{qu}^{(1)}]_{2311}$ and $[C_{qu}^{(1)}]_{2322}$ at 2 TeV. All other Wilson coefficients are assumed to vanish at 2 TeV

relations $C_S^{bs\mu\mu} = -C_P^{bs\mu\mu}$ (left) and $C_S^{\prime bs\mu\mu} = C_P^{\prime bs\mu\mu}$ (right). The most important constraint on these Wilson coefficients arises from the $B_s \to \mu^+\mu^-$ branching ratio. Mirror solutions in Wilson coefficient space that correspond to a mass eigenstate rate asymmetry $A_{\Delta\Gamma} \simeq -1 = -A_{\Delta\Gamma}^{\rm SM}$ are allowed by present data.

- The plots in Fig. 19 show scenarios with various combinatios of SMEFT Wilson coefficients. The left plot in Fig. 19 contains only tauonic Wilson coefficients, while the right plot shows a scenario with lepton flavour universal coefficients. The latter case is strongly constrained by electro-weak precision observables.
- Finally, Fig. 20 shows that the $b \to s\mu\mu$ anomalies can be explained by SMEFT 4-quark operators that enter the rare semi-leptonic decays at the loop level.

References

1. LHCb Collaboration, R. Aaij et al., Differential branching fractions and isospin asymmetries of $B \to K^{(*)}\mu^+\mu^-$ decays. JHEP **06**, 133 (2014). arXiv:1403.8044. https://doi.org/10.1007/JHEP06(2014)133
2. LHCb Collaboration, R. Aaij et al., Angular analysis and differential branching fraction of the decay $B_s^0 \to \phi\mu^+\mu^-$. JHEP **09**, 179 (2015). arXiv:1506.08777. https://doi.org/10.1007/JHEP09(2015)179
3. A. Bharucha, D.M. Straub, R. Zwicky, $B \to V\ell^+\ell^-$ in the Standard Model from light-cone sum rules. JHEP **08**, 098 (2016). https://doi.org/10.1007/JHEP08(2016)098. arXiv:1503.05534
4. R. R. Horgan, Z. Liu, S. Meinel, M. Wingate, Rare B decays using lattice QCD form factors. PoS Lattice **2014**, 372 (2015). arXiv:1501.00367. https://doi.org/10.22323/1.214.0372
5. N. Gubernari, A. Kokulu, D. van Dyk, $B \to P$ and $B \to V$ Form Factors from B-Meson Light-Cone Sum Rules beyond Leading Twist. JHEP **01**, 150 (2019). https://doi.org/10.1007/JHEP01(2019)150. arXiv:1811.00983
6. LHCb Collaboration, R. Aaij et al., Angular analysis of the $B^0 \to K^{*0}\mu^+\mu^-$ decay using 3 fb^{-1} of integrated luminosity. JHEP **02**, 104 (2016). arXiv:1512.04442. https://doi.org/10.1007/JHEP02(2016)104
7. ATLAS Collaboration, Angular analysis of $B_d^0 \to K^*\mu^+\mu^-$ decays in pp collisions at $\sqrt{s} = 8$ TeV with the ATLAS detector, Tech. Rep. ATLAS-CONF-2017-023, CERN, Geneva, Apr (2017)
8. CMS Collaboration, Measurement of the P_1 and P_5' angular parameters of the decay $B^0 \to K^{*0}\mu^+\mu^-$ in proton–proton collisions at $\sqrt{s} = 8\ TeV$. Tech. Rep. CMS-PAS-BPH-15-008, CERN, Geneva (2017)
9. CMS Collaboration, V. Khachatryan et al., Angular analysis of the decay $B^0 \to K^{*0}\mu^+\mu^-$ from pp collisions at $\sqrt{s} = 8$ TeV. Phys. Lett. B **753**, 424–448 (2016). arXiv:1507.08126. https://doi.org/10.1016/j.physletb.2015.12.020
10. A. Khodjamirian, T. Mannel, A.A. Pivovarov, Y.M. Wang, Charm-loop effect in $B \to K^{(*)}\ell^+\ell^-$ and $B \to K^*\gamma$. JHEP **09**, 089 (2010). https://doi.org/10.1007/JHEP09(2010)089. arXiv:1006.4945
11. C. Bobeth, M. Chrzaszcz, D. van Dyk, J. Virto, Long-distance effects in $B \to K^*\ell\ell$ from analyticity. Eur. Phys. J. C **78**, 451 (2018). https://doi.org/10.1140/epjc/s10052-018-5918-6. arXiv:1707.07305
12. LHCb Collaboration, R. Aaij et al., Test of lepton universality using $B^+ \to K^+\ell^+\ell^-$ decays, Phys. Rev. Lett. **113**, 151601 (2014). arXiv:1406.6482. https://doi.org/10.1103/PhysRevLett.113.151601
13. LHCb Collaboration, R. Aaij et al., Test of lepton universality with $B^0 \to K^{*0}\ell^+\ell^-$ decays. JHEP **08**, 055 (2017). arXiv:1705.05802. https://doi.org/10.1007/JHEP08(2017)055
14. M. Bordone, G. Isidori, A. Pattori, On the Standard Model predictions for R_K and R_{K^*}. Eur. Phys. J. C **76**, 440 (2016). https://doi.org/10.1140/epjc/s10052-016-4274-7. arXiv:1605.07633
15. BaBar Collaboration, J. P. Lees et al, Evidence for an excess of $\bar{B} \to D^{(*)}\tau^-\bar{\nu}_\tau$ decays, Phys. Rev. Lett. **109**, 101802 (2012). arXiv:1205.5442. https://doi.org/10.1103/PhysRevLett.109.101802
16. BaBar Collaboration, J. P. Lees et al., Measurement of an Excess of $\bar{B} \to D^{(*)}\tau^-\bar{\nu}_\tau$ Decays and Implications for Charged Higgs Bosons, Phys. Rev. D **88**, 072012 (2013). arXiv:1303.0571. https://doi.org/10.1103/PhysRevD.88.072012
17. Belle Collaboration, M. Huschle et al., Measurement of the branching ratio of $\bar{B} \to D^{(*)}\tau^-\bar{\nu}_\tau$ relative to $\bar{B} \to D^{(*)}\ell^-\bar{\nu}_\ell$ decays with hadronic tagging at Belle. Phys. Rev. D **92**, 072014 (2015). arXiv:1507.03233. https://doi.org/10.1103/PhysRevD.92.072014
18. Belle Collaboration, Y. Sato et al. Measurement of the branching ratio of $\bar{B}^0 \to D^{*+}\tau^-\bar{\nu}_\tau$ relative to $\bar{B}^0 \to D^{*+}\ell^-\bar{\nu}_\ell$ decays with a semileptonic tagging method. Phys. Rev. D **94**, 072007 (2016). arXiv:1607.07923. https://doi.org/10.1103/PhysRevD.94.072007
19. Belle Collaboration, S. Hirose et al., (2017), Measurement of the τ lepton polarization and $R(D^*)$ in the decay $\bar{B} \to D^*\tau^-\bar{\nu}_\tau$, Phys. Rev. Lett. **118**, 211801. arXiv:1612.00529. https://doi.org/10.1103/PhysRevLett.118.211801
20. LHCb Collaboration, R. Aaij et al., Measurement of the ratio of branching fractions $\mathcal{B}(\bar{B}^0 \to D^{*+}\tau^-\bar{\nu}_\tau)/\mathcal{B}(\bar{B}^0 \to D^{*+}\mu^-\bar{\nu}_\mu)$. Rev. Lett. **115**, 111803 (2015). arXiv:1506.08614. https://doi.org/10.1103/PhysRevLett.115.159901. https://doi.org/10.1103/PhysRevLett.115.159901. https://doi.org/10.1103/PhysRevLett.115.111803Phys
21. LHCb Collaboration, R. Aaij et al., Measurement of the ratio of the $B^0 \to D^{*-}\tau^+\nu_\tau$ and $B^0 \to D^{*-}\mu^+\nu_\mu$ branching fractions using three-prong τ-lepton decays. Phys. Rev. Lett. **120**, 171802 (2018). arXiv:1708.08856. https://doi.org/10.1103/PhysRevLett.120.171802
22. MILC Collaboration, J. A. Bailey et al., $B \to D\ell\nu$ form factors at nonzero recoil and $|V_{cb}|$ from 2+1-flavor lattice QCD. Phys. Rev. D **92**, 034506 (2015). arXiv:1503.07237. https://doi.org/10.1103/PhysRevD.92.034506
23. HPQCD Collaboration, H. Na, C. M. Bouchard, G. P. Lepage, C. Monahanand J. Shigemitsu, $B \to Dl\nu$ form factors atnonzero recoil and extraction of $|V_{cb}|$. Phys. Rev. D **92**, 054510 (2015). arXiv:1505.03925. https://doi.org/10.1103/PhysRevD.93.119906. https://doi.org/10.1103/PhysRevD.92.054510
24. F.U. Bernlochner, Z. Ligeti, M. Papucci, D.J. Robinson, Combined analysis of semileptonic B decays to D and D^*: $R(D^{(*)})$, $|V_{cb}|$, and new physics. Phys. Rev. D **95**, 115008 (2017). https://doi.org/10.1103/PhysRevD.95.115008,. arXiv:1703.05330, https://doi.org/10.1103/PhysRevD.97.059902
25. D. Bigi, P. Gambino, S. Schacht, $R(D^*)$, $|V_{cb}|$, and the heavy quark symmetry relations between form factors. JHEP **11**, 061 (2017). https://doi.org/10.1007/JHEP11(2017)061. arXiv:1707.09509
26. Belle Collaboration, A. Abdesselam et al., Precise determination of the CKM matrix element $|V_{cb}|$ with $\bar{B}^0 \to D^{*+}\ell^-\bar{\nu}_\ell$ decays with hadronic tagging at Belle. arXiv:1702.01521
27. Belle Collaboration, A. Abdesselam et al., Measurement of CKM Matrix Element $|V_{cb}|$ from $\bar{B} \to D^{*+}\ell^-\bar{\nu}_\ell$. arXiv:1809.03290

28. M. Jung, D.M. Straub, Constraining new physics in $b \to c\ell\nu$ transitions. JHEP **01**, 009 (2019). https://doi.org/10.1007/JHEP01(2019)009. arXiv:1801.01112
29. W. Altmannshofer, C. Niehoff, P. Stangl, D.M. Straub, Status of the $B \to K^*\mu^+\mu^-$ anomaly after Moriond 2017. Eur. Phys. J. C **77**, 377 (2017). https://doi.org/10.1140/epjc/s10052-017-4952-0. arXiv:1703.09189
30. W. Altmannshofer, P. Stangl, D.M. Straub, Interpreting hints for lepton flavor universality violation. Phys. Rev. D **96**, 055008 (2017). https://doi.org/10.1103/PhysRevD.96.055008. arXiv:1704.05435
31. B. Capdevila, A. Crivellin, S. Descotes-Genon, J. Matias, J. Virto, Patterns of New Physics in $b \to s\ell^+\ell^-$ transitions in the light of recent data. JHEP **01**, 093 (2018). https://doi.org/10.1007/JHEP01(2018)093. arXiv:1704.05340
32. L.-S. Geng, B. Grinstein, S. Jäger, J. Martin Camalich, X.-L. Ren, R.-X. Shi, Towards the discovery of new physics with lepton-universality ratios of $b \to s\ell\ell$ decays. Phys. Rev. D **96**, 093006 (2017). https://doi.org/10.1103/PhysRevD.96.093006. arXiv:1704.05446
33. M. Ciuchini, A.M. Coutinho, M. Fedele, E. Franco, A. Paul, L. Silvestrini et al., On Flavourful Easter eggs for New Physics hunger and Lepton Flavour Universality violation. Eur. Phys. J. C **77**, 688 (2017). https://doi.org/10.1140/epjc/s10052-017-5270-2. arXiv:1704.05447
34. T. Hurth, F. Mahmoudi, D. Martinez Santos, S. Neshatpour, Lepton nonuniversality in exclusive $b \to s\ell\ell$ decays. Phys. Rev. D **96**, 095034 (2017). https://doi.org/10.1103/PhysRevD.96.095034. arXiv:1705.06274
35. R. Alonso, B. Grinstein, J. Martin Camalich, Lepton universality violation and lepton flavor conservation in B-meson decays. JHEP **10**, 184 (2015). https://doi.org/10.1007/JHEP10(2015)184. arXiv:1505.05164
36. A. Greljo, G. Isidori, D. Marzocca, On the breaking of Lepton Flavor Universality in B decays. JHEP **07**, 142 (2015). https://doi.org/10.1007/JHEP07(2015)142. arXiv:1506.01705
37. R. Barbieri, G. Isidori, A. Pattori, F. Senia, Anomalies in B-decays and $U(2)$ flavour symmetry. Eur. Phys. J. C **76**, 67 (2016). https://doi.org/10.1140/epjc/s10052-016-3905-3. arXiv:1512.01560
38. L. Calibbi, A. Crivellin, T. Ota, Effective Field Theory Approach to $b \to s\ell\ell^{(\prime)}$, $B \to K^{(*)}\nu\bar{\nu}$ and $B \to D^{(*)}\tau\nu$ with Third Generation Couplings. Phys. Rev. Lett. **115**, 181801 (2015). https://doi.org/10.1103/PhysRevLett.115.181801. arXiv:1506.02661
39. M. Bauer, M. Neubert, Minimal Leptoquark Explanation for the $R_{D^{(*)}}$, R_K, and $(g-2)_\mu$ Anomalies. Phys. Rev. Lett. **116**, 141802 (2016). https://doi.org/10.1103/PhysRevLett.116.141802. arXiv:1511.01900
40. S. Fajfer, N. Košnik, Vector leptoquark resolution of R_K and $R_{D^{(*)}}$ puzzles. Phys. Lett. B **755**, 270–274 (2016). https://doi.org/10.1016/j.physletb.2016.02.018. arXiv:1511.06024
41. LHCb Collaboration, R. Aaij et al., Search for lepton-universality violation in $B^+ \to K^+\ell^+\ell^-$ decays, Phys. Rev. Lett. **122**, 191801 (2019). arXiv:1903.09252. https://doi.org/10.1103/PhysRevLett.122.191801
42. Belle Collaboration, A. Abdesselam et al., Test of lepton flavor universality in $B \to K^*\ell^+\ell^-$ decays at Belle. arXiv:1904.02440
43. B. Grinstein, D. Pirjol, Exclusive rare $B \to K^*\ell^+\ell^-$ decays at low recoil: Controlling the long-distance effects. Phys. Rev. D **70**, 114005 (2004). arXiv:hep-ph/0404250
44. M. Beylich, G. Buchalla, T. Feldmann, Theory of $B \to K^{(*)}\ell^+\ell^-$ decays at high q^2: OPE and quark-hadron duality. Eur. Phys. J. C **71**, 1635 (2011). https://doi.org/10.1140/epjc/s10052-011-1635-0. arXiv:1101.5118
45. S. Braß, G. Hiller, I. Nisandzic, Zooming in on $B \to K^*\ell\ell$ decays at low recoil. Eur. Phys. J. C **77**, 16 (2017). https://doi.org/10.1140/epjc/s10052-016-4576-9. arXiv:1606.00775
46. ATLAS Collaboration, M. Aaboud et al., (2018), Study of the rare decays of B_s^0 and B^0 mesons into muon pairs using data collected during 2015 and 2016 with the ATLAS detector, Submitted to: JHEP . arXiv:1812.03017
47. CMS Collaboration, S. Chatrchyan et al., Measurement of the B(s) to mu+ mu- branching fraction and search for B0 to mu+ mu- with the CMS experiment. Phys. Rev. Lett. **111**, 101804 (2013). https://doi.org/10.1103/PhysRevLett.111.101804. arXiv:1307.5025
48. CMS, LHCb Collaboration, V. Khachatryan et al., Observation of the rare $B_s^0 \to \mu^+\mu^-$ decay from the combined analysis of CMS and LHCb data. Nature **522**, 68–72 (2015). arXiv:1411.4413. https://doi.org/10.1038/nature14474
49. LHCb Collaboration, R. Aaij et al., Measurement of the $B_s^0 \to \mu^+\mu^-$ branching fraction and effective lifetime and search for $B^0 \to \mu^+\mu^-$ decays. Phys. Rev. Lett. **118**, 191801 (2017). arXiv:1703.05747. https://doi.org/10.1103/PhysRevLett.118.191801
50. Belle Collaboration, A. Abdesselam et al., Measurement of $\mathcal{R}(D)$ and $\mathcal{R}(D^*)$ with a semileptonic tagging method. arXiv:1904.08794
51. Belle Collaboration, G. Caria et al., Measurement of $\mathcal{R}(D)$ and $\mathcal{R}(D^*)$ with a semileptonic tagging method. arXiv:1910.05864
52. HFLAV Collaboration, Y. S. Amhis et al., Averages of b-hadron, c-hadron, and τ-lepton properties as of 2018. arXiv:1909.12524
53. J. Aebischer, J. Kumar, P. Stangl and D. M. Straub, A Global Likelihood for Precision Constraints and Flavour Anomalies. arXiv:1810.07698
54. D. M. Straub, flavio: a Python package for flavour and precision phenomenology in the Standard Model and beyond. arXiv:1810.08132
55. J. Aebischer, J. Kumar, D.M. Straub, Wilson: a Python package for the running and matching of Wilson coefficients above and below the electroweak scale. Eur. Phys. J. C **78**, 1026 (2018). https://doi.org/10.1140/epjc/s10052-018-6492-7. arXiv:1804.05033
56. W. Altmannshofer, P. Paradisi, D.M. Straub, Model-Independent Constraints on New Physics in $b \to s$ Transitions. JHEP **04**, 008 (2012). https://doi.org/10.1007/JHEP04(2012)008. arXiv:1111.1257
57. W. Altmannshofer, D.M. Straub, Cornering new physics in $b \to s$ transitions. JHEP **08**, 121 (2012). https://doi.org/10.1007/JHEP08(2012)121. arXiv:1206.0273
58. W. Altmannshofer, D.M. Straub, New physics in $B \to K^*\mu\mu$? Eur. Phys. J. C **73**, 2646 (2013). https://doi.org/10.1140/epjc/s10052-013-2646-9. arXiv:1308.1501
59. W. Altmannshofer, D.M. Straub, New physics in $b \to s$ transitions after LHC run 1. Eur. Phys. J. C **75**, 382 (2015). https://doi.org/10.1140/epjc/s10052-015-3602-7. arXiv:1411.3161
60. LHCb Collaboration, R. Aaij et al., Angular moments of the decay $\Lambda_b^0 \to \Lambda\mu^+\mu^-$ at low hadronic recoil. JHEP **09**, 146 (2018). arXiv:1808.00264. https://doi.org/10.1007/JHEP09(2018)146
61. LHCb Collaboration, R. Aaij et al., Differential branching fraction and angular analysis of $\Lambda^0\_b \to \Lambda\mu^+\mu^-$ decays. JHEP **06**, 115 (2015). arXiv:1503.07138. https://doi.org/10.1007/JHEP09(2018)145. https://doi.org/10.1007/JHEP06(2015)115
62. W. Detmold, S. Meinel, $\Lambda_b \to \Lambda\ell^+\ell^-$ form factors, differential branching fraction, and angular observables from lattice QCD with relativistic b quarks. Phys. Rev. D **93**, 074501 (2016). https://doi.org/10.1103/PhysRevD.93.074501. arXiv:1602.01399
63. S. Meinel, D. van Dyk, Using $\Lambda_b \to \Lambda\mu^+\mu^-$ data within a Bayesian analysis of $|\Delta B| = |\Delta S| = 1$ decays. Phys. Rev. D **94**, 013007 (2016). https://doi.org/10.1103/PhysRevD.94.013007. arXiv:1603.02974
64. A. Paul, D.M. Straub, Constraints on new physics from radiative B decays. JHEP **04**, 027 (2017). https://doi.org/10.1007/JHEP04(2017)027. arXiv:1608.02556

65. S. Descotes-Genon, T. Hurth, J. Matias, J. Virto, Optimizing the basis of $B \to K^* ll$ observables in the full kinematic range. JHEP **05**, 137 (2013). https://doi.org/10.1007/JHEP05(2013)137. arXiv:1303.5794
66. G. Hiller, M. Schmaltz, R_K and future $b \to s\ell\ell$ physics beyond the standard model opportunities. Phys. Rev. D **90**, 054014 (2014). https://doi.org/10.1103/PhysRevD.90.054014. arXiv:1408.1627
67. F. Sala, D.M. Straub, A new light particle in B decays? Phys. Lett. B **774**, 205–209 (2017). https://doi.org/10.1016/j.physletb.2017.09.072. arXiv:1704.06188
68. D. Ghosh, Explaining the R_K and R_{K^*} anomalies. Eur. Phys. J. C **77**, 694 (2017). https://doi.org/10.1140/epjc/s10052-017-5282-y. arXiv:1704.06240
69. A. Datta, J. Kumar, J. Liao, D. Marfatia, New light mediators for the R_K and R_{K^*} puzzles. Phys. Rev. D **97**, 115038 (2018). https://doi.org/10.1103/PhysRevD.97.115038. arXiv:1705.08423
70. W. Altmannshofer, M.J. Baker, S. Gori, R. Harnik, M. Pospelov, E. Stamou et al., Light resonances and the low-q^2 bin of R_{K^*}. JHEP **03**, 188 (2018). https://doi.org/10.1007/JHEP03(2018)188. arXiv:1711.07494
71. O. Catà, M. Jung, Signatures of a nonstandard Higgs boson from flavor physics. Phys. Rev. D **92**, 055018 (2015). https://doi.org/10.1103/PhysRevD.92.055018. arXiv:1505.05804
72. A. Celis, J. Fuentes-Martin, A. Vicente, J. Virto, Gauge-invariant implications of the LHCb measurements on lepton-flavor nonuniversality. Phys. Rev. D **96**, 035026 (2017). https://doi.org/10.1103/PhysRevD.96.035026. arXiv:1704.05672
73. J.E. Camargo-Molina, A. Celis, D.A. Faroughy, Anomalies in Bottom from new physics in Top. Phys. Lett. B **784**, 284–293 (2018). https://doi.org/10.1016/j.physletb.2018.07.051. arXiv:1805.04917
74. T. Hurth, S. Renner, W. Shepherd, Matching for FCNC effects in the flavour-symmetric SMEFT. arXiv:1903.00500
75. C. Bobeth, U. Haisch, New Physics in Γ_{12}^s: $(\bar{s}b)(\bar{\tau}\tau)$ Operators. Acta Phys. Polon. B **44**, 127–176 (2013). https://doi.org/10.5506/APhysPolB.44.127. arXiv:1109.1826
76. W. Altmannshofer, C. Niehoff, D.M. Straub, $B_s \to \mu^+\mu^-$ as current and future probe of new physics. JHEP **05**, 076 (2017). https://doi.org/10.1007/JHEP05(2017)076. arXiv:1702.05498
77. R. Alonso, B. Grinstein, J. Martin Camalich, $SU(2) \times U(1)$ gauge invariance and the shape of new physics in rare B decays. Phys. Rev. Lett. **113**, 241802 (2014). https://doi.org/10.1103/PhysRevLett.113.241802. arXiv:1407.7044
78. A. Arbey, T. Hurth, F. Mahmoudi, S. Neshatpour, Hadronic and New Physics Contributions to $b \to s$ Transitions. Phys. Rev. D **98**, 095027 (2018). https://doi.org/10.1103/PhysRevD.98.095027. arXiv:1806.02791
79. F. Beaujean, C. Bobeth, S. Jahn, Constraints on tensor and scalar couplings from $B \to K\bar{\mu}\mu$ and $B_s \to \bar{\mu}\mu$. Eur. Phys. J. C **75**, 456 (2015). https://doi.org/10.1140/epjc/s10052-015-3676-2. arXiv:1508.01526
80. M. Algueró, B. Capdevila, S. Descotes-Genon, P. Masjuan, J. Matias, Are we overlooking Lepton Flavour Universal New Physics in $b \to s\ell\ell$? arXiv:1809.08447
81. S. Jäger, J. Martin Camalich, On $B \to V\ell\ell$ at small dilepton invariant mass, power corrections, and new physics. JHEP **05**, 043 (2013). https://doi.org/10.1007/JHEP05(2013)043. arXiv:1212.2263
82. J. Lyon, R. Zwicky, Resonances gone topsy turvy—the charm of QCD or new physics in $b \to s\ell^+\ell^-$? arXiv:1406.0566
83. M. Ciuchini, M. Fedele, E. Franco, S. Mishima, A. Paul, L. Silvestrini et al., $B \to K^*\ell^+\ell^-$ decays at large recoil in the Standard Model: a theoretical reappraisal. JHEP **06**, 116 (2016). https://doi.org/10.1007/JHEP06(2016)116. arXiv:1512.07157
84. A. Khodjamirian, T. Mannel, Y.M. Wang, $B \to K\ell^+\ell^-$ decay at large hadronic recoil. JHEP **02**, 010 (2013). https://doi.org/10.1007/JHEP02(2013)010. arXiv:1211.0234
85. S. Descotes-Genon, L. Hofer, J. Matias, J. Virto, Global analysis of $b \to s\ell\ell$ anomalies. JHEP **06**, 092 (2016). https://doi.org/10.1007/JHEP06(2016)092. arXiv:1510.04239
86. A.K. Alok, B. Bhattacharya, D. Kumar, J. Kumar, D. London, S.U. Sankar, New physics in $b \to s\mu^+\mu^-$: distinguishing models through CP-violating effects. Phys. Rev. D **96**, 015034 (2017). https://doi.org/10.1103/PhysRevD.96.015034. arXiv:1703.09247
87. G. D'Amico, M. Nardecchia, P. Panci, F. Sannino, A. Strumia, R. Torre et al., Flavour anomalies after the R_{K^*} measurement. JHEP **09**, 010 (2017). https://doi.org/10.1007/JHEP09(2017)010. arXiv:1704.05438
88. E.E. Jenkins, A.V. Manohar, M. Trott, Renormalization group evolution of the standard model dimension six operators I: formalism and lambda dependence. JHEP **10**, 087 (2013). https://doi.org/10.1007/JHEP10(2013)087. arXiv:1308.2627
89. E.E. Jenkins, A.V. Manohar, M. Trott, Renormalization group evolution of the standard model dimension six operators II: Yukawa dependence. JHEP **01**, 035 (2014). https://doi.org/10.1007/JHEP01(2014)035. arXiv:1310.4838
90. R. Alonso, E.E. Jenkins, A.V. Manohar, M. Trott, Renormalization group evolution of the standard model dimension six operators III: Gauge coupling dependence and phenomenology. JHEP **04**, 159 (2014). https://doi.org/10.1007/JHEP04(2014)159. arXiv:1312.2014
91. J. Aebischer, M. Fael, C. Greub, J. Virto, B physics beyond the standard model at one loop: complete renormalization group evolution below the electroweak scale. JHEP **09**, 158 (2017). https://doi.org/10.1007/JHEP09(2017)158. arXiv:1704.06639
92. E.E. Jenkins, A.V. Manohar, P. Stoffer, Low-energy effective field theory below the electroweak scale: anomalous dimensions. JHEP **01**, 084 (2018). https://doi.org/10.1007/JHEP01(2018)084. arXiv:1711.05270
93. J. Aebischer et al., WCxf: an exchange format for Wilson coefficients beyond the Standard Model. Comput. Phys. Commun. **232**, 71–83 (2018). https://doi.org/10.1016/j.cpc.2018.05.022. arXiv:1712.05298
94. G. D'Ambrosio, G.F. Giudice, G. Isidori, A. Strumia, Minimal flavor violation: an effective field theory approach. Nucl. Phys. B **645**, 155–187 (2002). https://doi.org/10.1016/S0550-3213(02)00836-2. arXiv:hep-ph/0207036
95. A.J. Buras, J. Girrbach-Noe, C. Niehoff, D.M. Straub, $B \to K^{(*)}\nu\bar{\nu}$ decays in the standard model and beyond. JHEP **02**, 184 (2015). https://doi.org/10.1007/JHEP02(2015)184. arXiv:1409.4557
96. B. Grzadkowski, M. Iskrzynski, M. Misiak, J. Rosiek, Dimension-six terms in the standard model Lagrangian. JHEP **10**, 085 (2010). https://doi.org/10.1007/JHEP10(2010)085. arXiv:1008.4884
97. M. Ciuchini, A. M. Coutinho, M. Fedele, E. Franco, A. Paul, L. Silvestrini et al., New physics in $b \to s\ell^+\ell^-$ confronts new data on Lepton Universality. arXiv:1903.09632
98. A. Crivellin, C. Greub, D. Müller, F. Saturnino, Importance of loop effects in explaining the accumulated evidence for new physics in B decays with a vector leptoquark. Phys. Rev. Lett. **122**, 011805 (2019). https://doi.org/10.1103/PhysRevLett.122.011805. arXiv:1807.02068
99. S. Jäger, M. Kirk, A. Lenz, K. Leslie, Charming new physics in rare B-decays and mixing? Phys. Rev. D **97**, 015021 (2018). https://doi.org/10.1103/PhysRevD.97.015021. arXiv:1701.09183
100. C. Alpigiani et al., Unitarity Triangle Analysis in the Standard Model and Beyond, in 5th Large Hadron Collider Physics Con-

ference (LHCP 2017) Shanghai, China, May 15–20, 2017 (2017). arXiv:1710.09644
101. J. Aebischer, C. Bobeth, A. J. Buras, J.-M. Gérard, D. M. Straub, Master formula for ε'/ε beyond the Standard Model. arXiv:1807.02520
102. J. Aebischer, C. Bobeth, A.J. Buras, D.M. Straub, Anatomy of ε'/ε beyond the Standard Model. Eur. Phys. J. C **79**, 219 (2019). https://doi.org/10.1140/epjc/s10052-019-6715-6. arXiv:1808.00466
103. L. Di Luzio, A. Greljo, M. Nardecchia, Gauge leptoquark as the origin of B-physics anomalies. Phys. Rev. D **96**, 115011 (2017). https://doi.org/10.1103/PhysRevD.96.115011. arXiv:1708.08450
104. N. Assad, B. Fornal, B. Grinstein, Baryon number and lepton universality violation in leptoquark and diquark models. Phys. Lett. B **777**, 324–331 (2018). https://doi.org/10.1016/j.physletb.2017.12.042. arXiv:1708.06350
105. L. Calibbi, A. Crivellin, T. Li, Model of vector leptoquarks in view of the B-physics anomalies. Phys. Rev. D **98**, 115002 (2018). https://doi.org/10.1103/PhysRevD.98.115002. arXiv:1709.00692
106. M. Bordone, C. Cornella, J. Fuentes-Martin, G. Isidori, A three-site gauge model for flavor hierarchies and flavor anomalies. Phys. Lett. B **779**, 317–323 (2018). https://doi.org/10.1016/j.physletb.2018.02.011. arXiv:1712.01368
107. R. Barbieri, A. Tesi, B-decay anomalies in Pati-Salam SU(4). Eur. Phys. J. C **78**, 193 (2018). https://doi.org/10.1140/epjc/s10052-018-5680-9. arXiv:1712.06844
108. A. Greljo, B.A. Stefanek, Third family quark-lepton unification at the TeV scale. Phys. Lett. B **782**, 131–138 (2018). https://doi.org/10.1016/j.physletb.2018.05.033. arXiv:1802.04274
109. M. Blanke, A. Crivellin, B Meson Anomalies in a Pati-Salam Model within the Randall–Sundrum background. Phys. Rev. Lett. **121**, 011801 (2018). https://doi.org/10.1103/PhysRevLett.121.011801. arXiv:1801.07256
110. B. Fornal, S.A. Gadam, B. Grinstein, Left–right SU(4) vector leptoquark model for flavor anomalies. Phys. Rev. D **99**, 055025 (2019). https://doi.org/10.1103/PhysRevD.99.055025. arXiv:1812.01603
111. G. Hiller, D. Loose, K. Schönwald, Leptoquark flavor patterns & B decay anomalies. JHEP **12**, 027 (2016). https://doi.org/10.1007/JHEP12(2016)027. arXiv:1609.08895
112. B. Bhattacharya, A. Datta, J.-P. Guévin, D. London, R. Watanabe, Simultaneous explanation of the R_K and $R_{D^{(*)}}$ puzzles: a model analysis. JHEP **01**, 015 (2017). https://doi.org/10.1007/JHEP01(2017)015. arXiv:1609.09078
113. D. Buttazzo, A. Greljo, G. Isidori, D. Marzocca, B-physics anomalies: a guide to combined explanations. JHEP **11**, 044 (2017). https://doi.org/10.1007/JHEP11(2017)044. arXiv:1706.07808
114. A. Angelescu, D. Bečirevič, D.A. Faroughy, O. Sumensari, Closing the window on single leptoquark solutions to the B-physics anomalies. JHEP **10**, 183 (2018). https://doi.org/10.1007/JHEP10(2018)183. arXiv:1808.08179
115. J. Kumar, D. London, R. Watanabe, Combined Explanations of the $b \to s\mu^+\mu^-$ and $b \to c\tau^-\bar{\nu}$ anomalies: a general model analysis. Phys. Rev. D **99**, 015007 (2019). https://doi.org/10.1103/PhysRevD.99.015007. arXiv:1806.07403
116. J. Aebischer, A. Crivellin, C. Greub, QCD improved matching for semileptonic B decays with leptoquarks. Phys. Rev. D **99**, 055002 (2019). https://doi.org/10.1103/PhysRevD.99.055002. arXiv:1811.08907
117. S. Ferrara, M. Porrati, V.L. Telegdi, $g = 2$ as the natural value of the tree-level gyromagnetic ratio of elementary particles. Phys. Rev. D **46**, 3529–3537 (1992). https://doi.org/10.1103/PhysRevD.46.3529
118. R. Barbieri, C.W. Murphy, F. Senia, B-decay anomalies in a composite leptoquark model. Eur. Phys. J. C **77**, 8 (2017). https://doi.org/10.1140/epjc/s10052-016-4578-7. arXiv:1611.04930
119. J. Aebischer, A. Crivellin, M. Fael, C. Greub, Matching of gauge invariant dimension-six operators for $b \to s$ and $b \to c$ transitions. JHEP **05**, 037 (2016). https://doi.org/10.1007/JHEP05(2016)037. arXiv:1512.02830
120. E.E. Jenkins, A.V. Manohar, P. Stoffer, Low-Energy Effective Field Theory below the Electroweak Scale: Operators and Matching. JHEP **03**, 016 (2018). https://doi.org/10.1007/JHEP03(2018)016. arXiv:1709.04486
121. C. Cornella, J. Fuentes-Martin, G. Isidori, Revisiting the vector leptoquark explanation of the B-physics anomalies. arXiv:1903.11517
122. F. Feruglio, P. Paradisi, A. Pattori, Revisiting lepton flavor universality in B decays. Phys. Rev. Lett. **118**, 011801 (2017). https://doi.org/10.1103/PhysRevLett.118.011801. arXiv:1606.00524,
123. F. Feruglio, P. Paradisi, A. Pattori, On the importance of electroweak corrections for B anomalies. JHEP **09**, 061 (2017). https://doi.org/10.1007/JHEP09(2017)061. arXiv:1705.00929
124. D.A. Faroughy, A. Greljo, J.F. Kamenik, Confronting lepton flavor universality violation in B decays with high-p_T tau lepton searches at LHC. Phys. Lett. B **764**, 126–134 (2017). https://doi.org/10.1016/j.physletb.2016.11.011. arXiv:1609.07138
125. A. Greljo, D. Marzocca, High-p_T dilepton tails and flavor physics. Eur. Phys. J. C **77**, 548 (2017). https://doi.org/10.1140/epjc/s10052-017-5119-8. arXiv:1704.09015
126. B. Diaz, M. Schmaltz, Y.-M. Zhong, The leptoquark Hunter's guide: pair production. JHEP **10**, 097 (2017). https://doi.org/10.1007/JHEP10(2017)097. arXiv:1706.05033
127. A. Greljo, J. Martin Camalich, J. D. RuizÁ-lvarez, The Mono-Tau Menace: from B decays to high-p_T tails. arXiv:1811.07920
128. M. J. Baker, J. Fuentes-Martin, G. Isidori, M. König, High-pT signatures in vector-leptoquark models. arXiv:1901.10480
129. J. de Blas, J.C. Criado, M. Perez-Victoria, J. Santiago, Effective description of general extensions of the Standard Model: the complete tree-level dictionary. JHEP **03**, 109 (2018). https://doi.org/10.1007/JHEP03(2018)109. arXiv:1711.10391
130. P. P. Stangl, Direct constraints, flavor physics, and flavor anomalies in composite Higgs models. Ph.D. thesis, Munich, Tech. U., 2018. arXiv:1811.11750
131. ATLAS Collaboration, M. Aaboud et al., Search for low-mass resonances decaying into two jets and produced in association with a photon using pp collisions at $\sqrt{s} = 13$ TeV with the ATLAS detector, Submitted to: Phys. Lett. (2019) . arXiv:1901.10917
132. CMS Collaboration, A.M. Sirunyan et al., Search for narrow and broad dijet resonances in proton–proton collisions at $\sqrt{s} = 13$ TeV and constraints on dark matter mediators and other new particles. JHEP **08**, 130 (2018). https://doi.org/10.1007/JHEP08(2018)130. arXiv:1806.00843
133. C. Bobeth, M. Gorbahn, T. Hermann, M. Misiak, E. Stamou, M. Steinhauser, $B_{s,d} \to l^+l^-$ in the Standard Model with reduced theoretical uncertainty. Phys. Rev. Lett. **112**, 101801 (2014). https://doi.org/10.1103/PhysRevLett.112.101801. arXiv:1311.0903
134. M. Beneke, C. Bobeth, R. Szafron, Enhanced electromagnetic correction to the rare B-meson decay $B_{s,d} \to \mu^+\mu^-$. Phys. Rev. Lett. **120**, 011801 (2018). https://doi.org/10.1103/PhysRevLett.120.011801. arXiv:1708.09152
135. Flavour Lattice Averaging Group Collaboration, S. Aoki et al., FLAG review 2019. arXiv:1902.08191
136. M. Algueró, B. Capdevila, A. Crivellin, S. Descotes-Genon, P. Masjuan, J. Matias et al., Emerging patterns of new physics with and without Lepton Flavour Universal contributions. arXiv:1903.09578

137. A.K. Alok, A. Dighe, S. Gangal, D. Kumar, Continuing search for new physics in $b \to s\mu\mu$ decays: two operators at a time. JHEP **06**, 089 (2019). https://doi.org/10.1007/JHEP06(2019)089. arXiv:1903.09617
138. K. Kowalska, D. Kumar, E. M. Sessolo, Implications for New Physics in $b \to s\mu\mu$ transitions after recent measurements by Belle and LHCb. arXiv:1903.10932
139. A. Arbey, T. Hurth, F. Mahmoudi, D. M. Santos, S. Neshatpour, Update on the $b \to s$ anomalies. arXiv:1904.08399
140. A.J. Buras, Relations between $\Delta M_{s,d}$ and $B_{s,d} \to \mu\bar{\mu}$ in models with minimal flavor violation. Phys. Lett. B **566**, 115–119 (2003). https://doi.org/10.1016/S0370-2693(03)00561-6. arXiv:hep-ph/0303060
141. M. Blanke, A.J. Buras, Lower bounds on $\Delta M(s,d)$ from constrained minimal flavour violation. JHEP **05**, 061 (2007). https://doi.org/10.1088/1126-6708/2007/05/061. arXiv:hep-ph/0610037
142. W. Altmannshofer, A.J. Buras, D. Guadagnoli, The MFV limit of the MSSM for low tan(beta): Meson mixings revisited. JHEP **11**, 065 (2007). https://doi.org/10.1088/1126-6708/2007/11/065. arXiv:hep-ph/0703200
143. L. Di Luzio, M. Kirk, A. Lenz, Updated B_s-mixing constraints on new physics models for $b \to s\ell^+\ell^-$ anomalies. Phys. Rev. D **97**, 095035 (2018). https://doi.org/10.1103/PhysRevD.97.095035. arXiv:1712.06572